

คุณลักษณะของถ่านกัมมันต์ที่ได้จากกากของรำข้าวและการประยุกต์ใช้เป็นตัวรองรับของตัวเร่ง
ปฏิกิริยา



นาย เบนจพล นิธิเจริญวงศ์

ศูนย์วิทยทรัพยากร จุฬาลงกรณ์มหาวิทยาลัย

วิทยานิพนธ์นี้เป็นส่วนหนึ่งของการศึกษาตามหลักสูตรปริญญาวิศวกรรมศาสตรมหาบัณฑิต

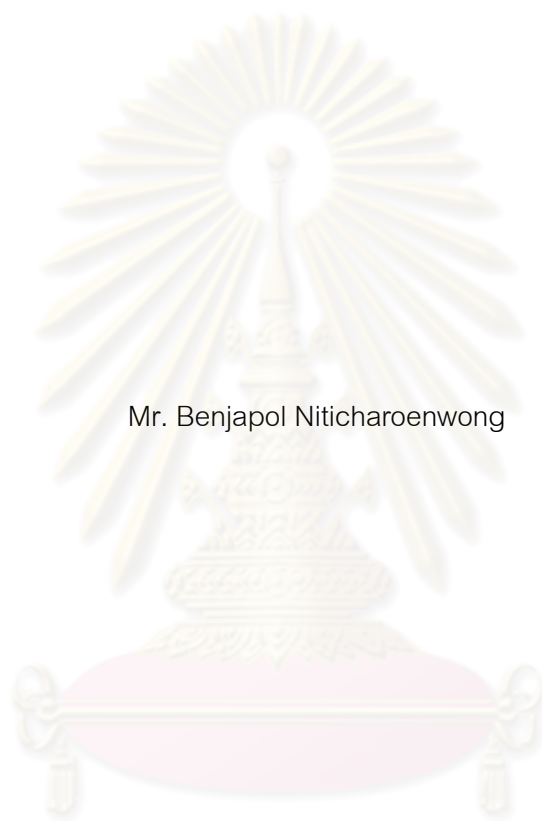
สาขาวิชาวิศวกรรมเคมี ภาควิชาวิศวกรรมเคมี

คณะวิศวกรรมศาสตร์ จุฬาลงกรณ์มหาวิทยาลัย

ปีการศึกษา 2553

ลิขสิทธิ์ของจุฬาลงกรณ์มหาวิทยาลัย

CHARACTERISTICS OF ACTIVATED CARBON DERIVED FROM RICE BRAN RESIDUES
AND ITS APPLICATION AS A CATALYST SUPPORT



Mr. Benjapol Niticharoenwong

ศูนย์วิทยทรัพยากร
จุฬาลงกรณ์มหาวิทยาลัย
A Thesis Submitted in Partial Fulfillment of the Requirements
for the Degree of Master of Engineering Program in Chemical Engineering

Department of Chemical Engineering

Faculty of Engineering

Chulalongkorn University

Academic Year 2010

Copyright of Chulalongkorn University

เบญจพล นิธิเจริญวงศ์ : คุณลักษณะของถ่านกัมมันต์ที่ได้จากกากของรำข้าวและการประยุกต์ใช้เป็นตัวรองรับของตัวเร่งปฏิกิริยา. (CHARACTERISTICS OF ACTIVATED CARBON DERIVED FROM RICE BRAN RESIDUES AND ITS APPLICATION AS A CATALYST SUPPORT)

อ. ที่ปรึกษาวิทยานิพนธ์หลัก: รศ.ดร. บรรเจิด จงสมจิตร, 84 หน้า.

งานวิจัยนี้เน้นศึกษาเกี่ยวกับคุณลักษณะของถ่านกัมมันต์ที่ได้จากกากของรำข้าวโดยใช้วิธีการกระตุ้นด้วยสารเคมี (ซิงก์คลอไรด์และฟอสฟอริก แอซิดเป็นสารกระตุ้น) ที่อุณหภูมิต่างๆ และศึกษาเกี่ยวกับประสิทธิภาพของการใช้ถ่านกัมมันต์เป็นตัวรองรับของตัวเร่งปฏิกิริยาโคบอลต์ในปฏิกิริยาไฮโดรจิเนชันของคาร์บอนไดออกไซด์ จากการทดลองพบว่า ถ่านกัมมันต์ที่ได้จากกากของรำข้าวโดยใช้วิธีการกระตุ้นด้วยสารเคมีให้พื้นที่ผิวจำเพาะสูง เมื่อเปรียบเทียบผลระหว่างสารกระตุ้น พบว่า การใช้ซิงก์คลอไรด์เป็นสารกระตุ้นให้พื้นที่ผิวจำเพาะสูงกว่าการใช้ฟอสฟอริก แอซิดเป็นสารกระตุ้น นอกจากนี้ถ่านกัมมันต์ที่ได้จากการกระตุ้นด้วยสารเคมียังแสดงลักษณะรูพรุนแบบไมโครพอร์รัล (ขนาดรูพรุนเล็กกว่า 2 นาโนเมตร) เป็นส่วนมากและแบบมีโซพอร์รัล (ขนาดรูพรุนอยู่ระหว่าง 2 ถึง 50 นาโนเมตร) เพียงบางส่วน เมื่อนำถ่านกัมมันต์เหล่านี้ไปใช้เป็นตัวรองรับของตัวเร่งปฏิกิริยาโคบอลต์ในปฏิกิริยาไฮโดรจิเนชันของคาร์บอนไดออกไซด์ พบว่า ประสิทธิภาพของการใช้ถ่านกัมมันต์เป็นตัวรองรับของตัวเร่งปฏิกิริยาโคบอลต์ค่อนข้างต่ำ อาจจะเนื่องมาจากสิ่งเจือปนซึ่งตกค้างอยู่บนถ่านกัมมันต์ นั่นคือซัลเฟอร์

ศูนย์วิทยทรัพยากร
จุฬาลงกรณ์มหาวิทยาลัย

ภาควิชา วิศวกรรมเคมี
สาขาวิชา วิศวกรรมเคมี
ปีการศึกษา 2553

ลายมือชื่อนิติศ.....เบญจพล นิธิเจริญวงศ์.....
ลายมือชื่อ อ.ที่ปรึกษาวิทยานิพนธ์หลัก. *Asst. Prof. Dr. Jit*

5270368021 : MAJOR CHEMICAL ENGINEERING

KEYWORDS : ACTIVATED CARBON / DEOIL RICE BRAN / CHEMICAL ACTIVATION
/ CO₂ HYDROGENATION / COBALT CATALYST

BENJAPOL NITICHAROENWONG : CHARACTERISTICS OF ACTIVATED
CARBON DERIVED FROM RICE BRAN RESIDUES AND ITS APPLICATION
AS A CATALYST SUPPORT.

THESIS ADVISOR : ASSOC. PROF. BUNJERD JONGSOMJIT, Ph.D., 84 pp.

This research focuses on investigation of the characteristics of activated carbons from deoil rice bran by using chemical activation (ZnCl₂ and H₃PO₄ as activating agent) at different temperatures and performance of activated carbon used as catalyst support for cobalt catalyst in CO₂ hydrogenation. It was found that the high surface area of activated carbon obtains from rice bran residues can be achieved by using chemical activation that the ZnCl₂ activation, which was higher than that obtained by H₃PO₄ activation. In addition, the activated carbons for both H₃PO₄ and ZnCl₂ activations exhibited a combination of mostly microporous and partly mesoporous structure. Then, these activated carbons were used as catalyst support for cobalt catalyst in CO₂ hydrogenation. It was found that the performance obtained from using these activated carbons as supports of Co catalysts are poor probably due to amounts of sulfur impurity left from using H₂SO₄ for treating at the beginning for preparation of activated carbon.

Department : Chemical Engineering.....
Field of Study : Chemical Engineering.....
Academic Year : 2010.....

Student's Signature เบนจพล นิติเจริญวงศ์
Advisor's Signature Bunjerd Jongsomjit

ACKNOWLEDGEMENTS

The author would like to express greatest gratitude to his advisor, Associate Professor Bunjerd Jongsomjit on his invaluable suggestion and guidance throughout of this study. Without the continuous guidance and comments, this work would never have been achieved. In addition, I would be also grateful to thank to Assistant Professor Anongnat Somwangthanaroj who has been the chairman of the committee for this thesis, and Assistant Professor Joongjai Panpranot, Assistant Professor Okorn Mekasuwandamrong, members of the thesis committee for their kind cooperation.

Most of all, the author would like to express his highest gratitude to his parents who always pay attention to his all the times for their suggestions and have provided support and encouragements. The most success of graduation is devoted to his parents.

Moreover, the author wishes to thank all my friends and members of the Center of Excellent on Catalysis & Catalytic Reaction Engineering, Department of Chemical Engineering, Chulalongkorn University for their assistance and friendly encouragement. To the others, not specifically named, who have provided his with support and encouragement, please be assured that he thinks of you.

Finally, the author would like to thank the Thailand Research Fund (TRF), as well as the Graduate School of Chulalongkorn University for their Financial Supports.

ศูนย์วิทยทรัพยากร
จุฬาลงกรณ์มหาวิทยาลัย

CONTENTS

	page
ABSTRACT (THAI).....	iv
ABSTRACT (ENGLISH).....	v
ACKNOWLEDGEMENTS.....	vi
CONTENTS.....	vii
LIST OF TABLES.....	xi
LIST OF FIGURES.....	xii
LIST OF SCHEMES.....	xiv
CHAPTER	
I. INTRODUCTION.....	1
1.1 Rationale.....	1
1.2 Objective.....	3
1.3 Research scope.....	3
1.4 Research methodology.....	4
II. THEORY.....	5
2.1 Activated carbon.....	5
2.2 Cobalt.....	9
2.3 Cobalt Oxides.....	12
2.4 CO ₂ hydrogenation.....	12
III. LITERATURE REVIEW.....	14
3.1 Activated carbon from other precursors.....	14
3.2 Activated carbon from rice bran.....	15
3.3 Co catalyst.....	15
3.4 CO ₂ Hydrogenation Reactions.....	18
3.5 Co/AC catalysts.....	22
IV. EXPERIMENTAL.....	27
4.1 Preparation activated carbon.....	27
4.1.1 Chemical.....	27

4.1.2 Experimental procedure.....	27
4.2 Cobalt Loading.....	28
4.3 Catalyst Nomenclature.....	28
4.4 Catalyst Characterization.....	29
4.4.1 Proximate analysis.....	29
4.4.2 Elemental analyzer.....	29
4.4.3 X-ray diffraction (XRD).....	30
4.4.4 N ₂ Physisorption.....	30
4.4.5 CO Chemisorptions.....	30
4.4.6 Temperature-programmed reduction (TPR).....	30
4.4.7 X-ray photoelectron spectroscopy (XPS).....	30
4.4.8 Transmission Electron Microscopy (TEM).....	31
4.4.9 Thermal Gravimetric Analysis (TGA).....	31
4.4.10 Scanning Electron Microscopy (SEM) and Energy Dispersive X-ray Spectroscopy (EDX).....	31
4.4.11 X-ray fluorescence spectrometry (XRF).....	31
4.4.12 Inductive Coupled Plasma Optical Emission Spectrometer (ICP-OES).....	31
4.5 Reaction study in CO ₂ hydrogenation.....	32
4.5.1 Materials.....	32
4.5.2 Apparatus.....	32
4.5.2.1 Reactor.....	32
4.5.2.2 Automation Temperature Controller.....	32
4.5.2.3 Electrical Furnace.....	32
4.5.2.4 Gas Controlling System.....	32
4.5.2.5 Gas Chromatography.....	32
4.5.3 Procedures.....	33
V. RESULTS AND DISCUSSION.....	36
5.1 Characteristics of activated carbon derived from deoil rice bran residues under chemical activation.....	36
5.1.1 Characteristics of rice bran residues.....	36

5.1.2 Analysis of BET surface area and pore structure.....	37
5.1.3 Analysis of yield.....	41
5.1.4 Analysis of XRD.....	42
5.1.5 Analysis of Scanning Electron Microscopy.....	43
5.1.6 Analysis of Thermal Gravimetric Analysis.....	44
5.1.7 Analysis of impurity of activated carbons.....	47
5.2 Comparison of catalytic activity between Co-catalyst on various activated carbons For CO ₂ hydrogenation.....	47
5.2.1 Analysis of BET surface area and pore structure.....	48
5.2.2 Analysis of CO Chemisorption.....	48
5.2.3 Analysis of Scanning Electron Microscopy (SEM) and Energy Dispersive X-ray Spectroscopy (EDX).....	49
5.2.4 Analysis of Transmission Electron Microscopy (TEM).....	51
5.2.5 Analysis of X-ray diffraction (XRD).....	53
5.2.6 Analysis of X-ray photoelectron spectroscopy.....	54
5.2.7 Analysis of Thermal Gravimetric Analysis.....	60
5.2.8 Analysis of Temperature-programmed reduction (TPR).....	61
5.2.9 Study of CO ₂ hydrogenation.....	63
VI. CONCLUSIONS AND RECOMMENDATIONS.....	66
6.1 Conclusions.....	66
6.1.1 Characteristics of activated carbon derived from deoil rice bran residues under chemical activation.....	66
6.1.2 Comparison of catalytic activity between Co catalysts on various activated carbons For CO ₂ hydrogenation.....	66
6.2 Recommendations.....	67
REFERENCES.....	68
APPENDICES.....	74
APPENDICES A: CALCULATION FOR CATALYST PREPARATION.....	75
APPENDICES B: CALCULATION FOR TOTAL CO CHEMISSORPTION AND DISPERSION.....	76
APPENDICES C: CALCULATION OF TURNOVER OF FREQUENCY.....	78

APPENDICES D: CALIBRATION CURVES.....	79
APPENDICES E: CALCULATION OF CO ₂ CONVERSION, REACTION RATE AND SELECTIVITY.....	82
APPENDICES F: REVERSE WATER GAS SHIFT (RWGS) REACTION.....	83
VITA.....	84



ศูนย์วิทยทรัพยากร
จุฬาลงกรณ์มหาวิทยาลัย

LIST OF TABLES

Table		Page
2.1	Physical properties of cobalt.....	10
3.1	Comparisons of the characteristics of porosity of other literature data for other precursors under optimum condition.....	14
4.1	Operating condition for gas chromatograph.....	33
5.1	Proximate analysis results of deoil rice bran.....	36
5.2	Elemental composition of deoil rice bran.....	36
5.3	Pore characteristics for activated carbons.....	41
5.4	The impurity of activated carbons.....	49
5.5	BET surface area, pore volume and average pore sizes of the Co- catalysts.....	50
5.6	Active site, total CO-chemisorptions and %Co dispersion of the Co- catalysts.....	51
5.7	EDX analysis of cobalt catalysts.....	53
5.8	The binding energy and FWHM of Co.....	59
5.9	The conversion, reaction rate, product selectivity and TOF during CO ₂ hydrogenation for Co catalysts.....	64
D.1	Conditions use in Shimadzu modal GC-8A and GC-14B.....	79

LIST OF FIGURES

Figure		Page
1.1	Structure of rice.....	1
3.1	Proposed decomposition procedure of Co(II) acetate on SiO ₂	16
3.2	Proposed reduction procedure of Co species of Co(II)-Re/SiO ₂	17
3.3	Proposal reduction procedure of Co(II)acetate, Co(II)nitrate/Co(II)acetate on silica during catalyst preparation; a: Co(II)acetate; b: cobalt(II)nitrate/cobalt(II)acetate.....	17
3.4	Proposed mechanism for the heterogeneous catalytic hydrogenation of CO ₂ to methanol.....	19
3.5	The reaction mechanisms proposed for C, CO and CO ₂ hydrogenation	20
3.6	Proposed mechanism of CO formation from CO ₂ and H ₂ on Cu/K/SiO ₂ catalyst.....	22
5.1	Effect of activation temperature on the surface area of activated carbons.....	38
5.2	Adsorption-desorption isotherm of activated carbons at different activation temperature.....	40
5.3	Pore size distribution of activated carbons by Horvath-Kawazoe method.....	42
5.4	Effect of activation temperature on the yield of activated carbons.....	43
5.5	X-ray diffractogram of activated carbon at the different activation temperature and raw material.....	44
5.6	Scanning electron micrographs of activated carbons.....	45
5.7	TG and DTG thermograms of activated carbons.....	48
5.8	SEM/EDX images of Co-catalysts.....	53
5.9	TEM images of Ru-promoted Co-catalysts.....	54
5.10	XRD patterns of Co catalysts.....	55
5.11	The deconvolution of Co2p _{3/2} of XPS spectra of Co-catalysts.....	58
5.12	TG and DTG thermograms of Co catalysts.....	61

Figure		Page
5.13	Reduction behaviors of the Co-catalysts.....	62
5.14	The rate vs. time on stream of the cobalt catalysts.....	65
D.1	The calibration curve of carbon dioxide.....	73
D.2	The calibration curve of carbon monoxide.....	73
D.3	The calibration curve of methane.....	74
D.4	The calibration curve of ethane.....	74



ศูนย์วิทยทรัพยากร
จุฬาลงกรณ์มหาวิทยาลัย

LIST OF SCHEMES

Scheme		Page
1.1	Diagram of research methodology.....	4
4.1	Flow diagram of CO ₂ hydrogenation system.....	35



ศูนย์วิทยทรัพยากร
จุฬาลงกรณ์มหาวิทยาลัย

CHAPTER I

INTRODUCTION

1.1 Rationale

Rice bran (Figure 1.1) is a by-product of rice milling process, the conversion of brown rice to white rice. It is obtained from the outer layers of the brown rice during milling. In a few years ago, this by-product was increasingly considered as it contains various compounds that impart beneficial effect on human health. So, it is usually extracted oil or is sometimes extracted



Figure1.1 Structure of rice

other compounds, such as protein to be nutrient for human. Finally, it only remains residues that are usually led to waste or animal feed. Therefore, leading the rice bran residues apply to activated carbon can increase a value of material and is a very interesting topic. This research focuses on using rice bran residue, which was extracted oil, called deoil rice bran, to obtain the activated carbons that were applied as a catalyst support.

Activated carbon is a well known material used in many applications on an industrial scale. For example, it was used for the purification of gases (Guo and Lue, 2002), the removal of organic pollutants from water (Zhou, Wang, and Chi, 2009), the removal of heavy metal from waste water (Daifullah et al., 2003), as a catalyst or a catalyst support in the catalytic process (Bedia, 2010; Gu, 2010), etc. So, the activated carbon has an important role in many industries.

In principle, the methods of preparing an activated carbon can be divided into two categories : physical activation and chemical activation (Ahmadpour and Do, 1996). In the physical activation, a raw material is first carbonized and the carbonized material is secondary activated by steam (Li et al., 2008), carbon dioxide (Guo et al., 2009), air (Wei et al., 2006) or their mixture i.e. there are two steps: carbonization step and activation step. In the chemical activation, a raw material is impregnated with an activation agent and an impregnated material is heat-treated under inert atmosphere. The carbonization step and activation step are carried out simultaneously in the chemical activation process (Guo, 2002; Kalderis, 2008; Basta, 2009; Liou, 2009). However, sometime the methods for preparing an activated carbon is modified (such as chemical activation followed by physical activation (Azevedo et al., 2007)) to improve characteristics of activated carbon such as surface area, pore volume, etc.

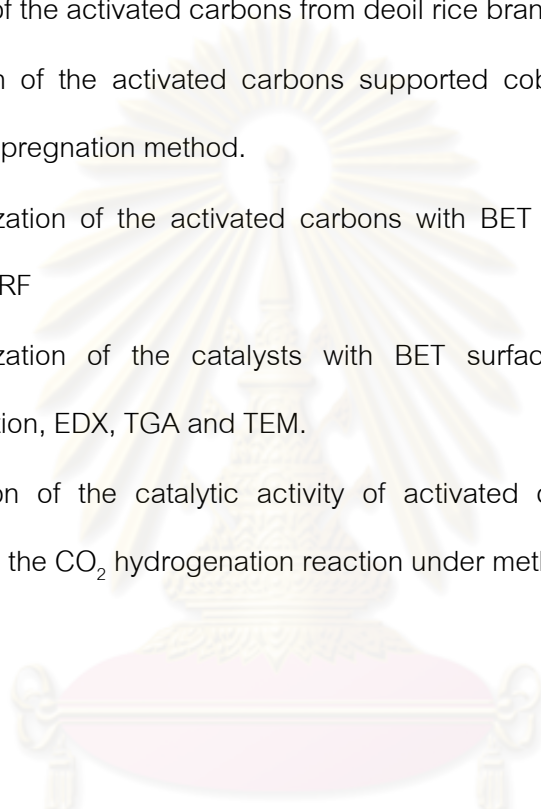
In many years later, activated carbons were often produced from the carbonaceous material such as coconut shell (Li, 2008; Guo, 2009), rice husk (Liou and Wu, 2009), and etc. However, there are few reports on the preparation of activated carbon from rice bran (Suzuki, 2007; Kumar, 2009). Therefore, in this study, rice bran residues or deoil rice brans have been used as the activated carbon precursor. The characteristics of activated carbons prepared from deoil rice bran are investigated and used as catalyst support for cobalt catalyst in CO₂ hydrogenation.

1.2 Objective

1. To investigate characteristics of activated carbons derived from deoil rice brans.
2. To investigate performance of activated carbon, prepared from deoil rice bran, that is used as catalyst support for cobalt catalyst in CO₂ hydrogenation.

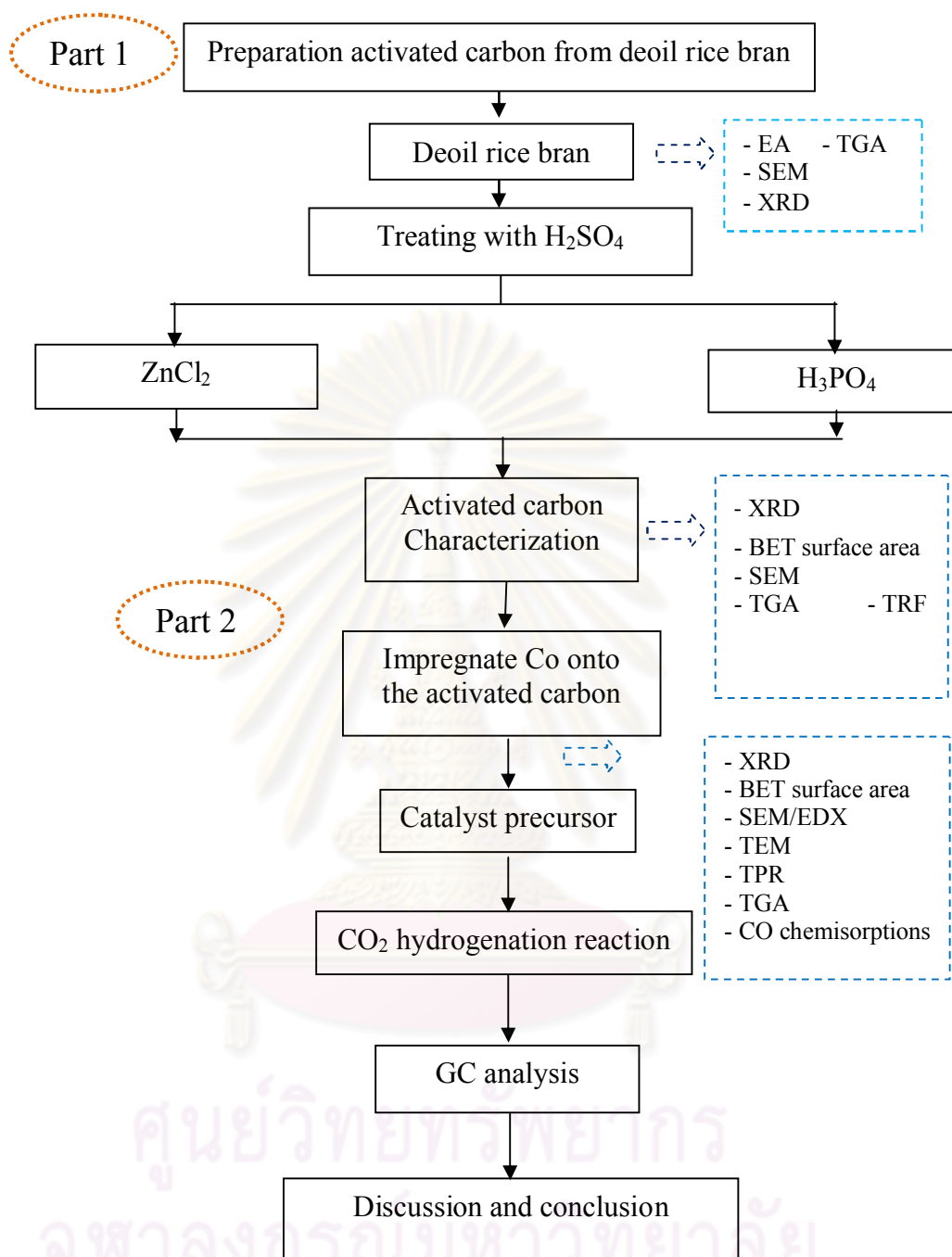
1.3 Research scope

- Synthesis of the activated carbons from deoil rice brans.
- Preparation of the activated carbons supported cobalt catalysts by incipient wetness impregnation method.
- Characterization of the activated carbons with BET surface area, XRD, TGA, SEM and TRF
- Characterization of the catalysts with BET surface area, XRD, TPR, CO chemisorption, EDX, TGA and TEM.
- Investigation of the catalytic activity of activated carbons supported-cobalt catalysts in the CO₂ hydrogenation reaction under methanation conditions.



ศูนย์วิทยทรัพยากร
จุฬาลงกรณ์มหาวิทยาลัย

1.4 Research Methodology



Scheme 1.1 Diagram of research methodology

CHAPTER II

THEORY

2.1 Activated carbon

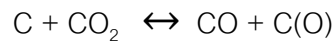
Activated carbon, also called activated charcoal or activated coal is a form of carbon that has been processed to make it extremely porous and thus to have a very large surface area available for adsorption or chemical reactions. The word activated in the name is sometimes replaced with active. Due to its high degree of microporosity, just 1 gram of activated carbon has a surface area in excess of 500 m². Sufficient activation for useful applications may come solely from the high surface area, though further chemical treatment often enhances the absorbing properties of the material.

Activated carbon is carbon produced from carbonaceous source materials like coconut shells, peat, wood, coir, lignite, coal and petroleum pitch. It can be produced by one of the following processes: physical activation, chemical activation or combine of physical and chemical activation to obtain a desired activated carbon.

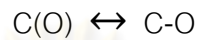
Physical activation : The precursor is developed into activated carbons using gases. This is generally done by using one or a combination of the following processes:

- *Carbonization* : Material with carbon content is pyrolyzed at temperatures in the range 600–900 °C, in absence of air (usually in inert atmosphere with gases like argon or nitrogen).
- *Activation/Oxidation* : Raw material or carbonised material is exposed to oxidizing atmospheres by the gasifying agent(carbon dioxide, oxygen, or steam) at temperatures above 250 °C, usually in the temperature range of 600–1200 °C. These agents extract carbon atoms from the structure of the porous carbon according to the following equations.

For the C-CO₂ reaction the mechanism is postulated to be :



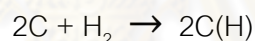
In which a surface oxygen complex [C(O)] is initially formed, subsequently becoming stable under the reaction conditions and acting as a retardant by blocking reaction sites:



It may, however, decompose leaving the surface as CO,



Involving the use of steam(water vapor), hydrogen is similarly chemisorbed on the carbon surface, where C(H) describes hydrogen chemisorbed on a carbon surface :



Summarizing, the activation reactions result in (a) the opening of porosity which, originally, was not accessible to an adsorbate; (b) the enhancement of micropore volumes and (c) widening of micropores into the mesopore range.

Chemical activation : Prior to carbonization, the raw material is impregnated with certain chemicals. The chemical is typically an acid, strong base, or a salt (phosphoric acid, potassium hydroxide, sodium hydroxide, zinc chloride, respectively). Then, the raw material is carbonized at lower temperatures (450–900 °C). It is believed that the carbonization / activation step proceeds simultaneously with the chemical activation. This technique can be problematic in some cases, for example, zinc trace residues may remain in the end product. However, chemical activation is preferred over physical activation owing to the lower temperatures and shorter time needed for activating material.

Effects of impregnations (chemical activation) :

for activation with ZnCl_2 , (a) the volume of micropores developed is similar to the volume of zinc chloride introduced into the particle, and the microporosity is uniform and (b) zinc chloride acts at temperatures $< 500^\circ\text{C}$.

for activation with H_3PO_4 , (a) the volume of micropores developed during activation is similar to the volume of the acid used in the impregnation of the precursor, the heterogeneity of the microporosity being constant in all carbons and (b) phosphoric acid acts at temperatures $< 450^\circ\text{C}$ leading to highly activated carbon.

for activation with KOH , (a) the reactant acts after the pyrolysis of the precursor, at temperatures above 700°C ; (b) the development of porosity relates to the extent of impregnation by the KOH ; (c) initially, narrow microporosity is formed followed by the wider microporosity at the expense of the narrow microporosity ; (d) activation can proceed without disintegration to form powder and (e) high ratios of KOH to carbon result in the disintegration of the carbon granules to powder.

A principal conclusion is that chemical activation produces similar or higher porosity than does physical activation. There are two advantages to the use of chemical activation methods namely (a) higher yields, 27-47 wt% compared with 6 wt% for physical activation and (b) the surfaces of the activated fibers prepared by chemical activation are less damaged.

Under an electron microscope, the high surface-area structures of activated carbon are revealed. Individual particles are intensely convoluted and display various kinds of porosity; there may be many areas where flat surfaces of graphite-like material run parallel to each other.

Activated carbons are complex products which are difficult to classify on the basis of their behaviour, surface characteristics and preparation methods. However, some broad classification is made for general purpose based on their physical characteristics.

Powdered activated carbon (PAC) : Traditionally, active carbons are made in particular form as powders or fine granules less than 1.0 mm in size with an average diameter between .15 and .25 mm. Thus they present a large surface to volume ratio with a small diffusion distance. PAC is made up of crushed or ground carbon particles, 95–100% of which will pass through a designated mesh sieve or sieve. Granular activated carbon is defined as the activated carbon being retained on a 50-mesh sieve (0.297 mm) and PAC material as finer material. PAC is not commonly used in a dedicated vessel, owing to the high head loss that would occur. PAC is generally added directly to other process units, such as raw water intakes, rapid mix basins, clarifiers, and gravity filters.

Granular activated carbon (GAC): Granular activated carbon has a relatively larger particle size compared to powdered activated carbon and consequently, presents a smaller external surface. Diffusion of the adsorbate is thus an important factor. These carbons are therefore preferred for all adsorption of gases and vapors as their rate of diffusion are faster. Granulated carbons are used for water treatment, deodorization and separation of components of flow system. GAC can be either in the granular form or extruded. GAC is designated by sizes such as 8×20, 20×40, or 8×30 for liquid phase applications and 4×6, 4×8 or 4×10 for vapor phase applications. A 20×40 carbon is made of particles that will pass through a U.S. Standard Mesh Size No. 20 sieve (0.84 mm) (generally specified as 85% passing) but be retained on a U.S. Standard Mesh Size No. 40 sieve (0.42 mm) (generally specified as 95% retained). The most popular aqueous phase carbons are the 12×40 and 8×30 sizes because they have a good balance of size, surface area, and head loss characteristics.

Extruded activated carbon (EAC): Extruded activated carbon combines powdered activated carbon with a binder, which are fused together and extruded into a cylindrical shaped activated carbon block with diameters from 0.8 to 130 mm. These are mainly used for gas phase applications because of their low pressure drop, high mechanical strength and low dust content.

Impregnated carbon: Porous carbons containing several types of inorganic impregnate such as iodine, silver, cations such as Al, Mn, Zn, Fe, Li, Ca have also been prepared

for specific application in air pollution control especially in museums and galleries. Due to antimicrobial/antiseptic properties, silver loaded activated carbon is used as an adsorbent for purification of domestic water. Drinking water can be obtained from natural water by treating the natural water with a mixture of activated carbon and $\text{Al}(\text{OH})_3$, a flocculating agent. Impregnated carbons are also used for the adsorption of H_2S and thiols. Adsorption rates for H_2S as high as 50% by weight have been reported.

Polymer coated carbon : This is a process by which a porous carbon can be coated with a biocompatible polymer to give a smooth and permeable coat without blocking the pores. The resulting carbon is useful for hemoperfusion. Hemoperfusion is a treatment technique in which large volumes of the patient's blood are passed over an adsorbent substance in order to remove toxic substances from the blood.

Other : Activated carbon is also available in special forms such as cloths and fibres. The "carbon cloth" for instance is used in personnel protection for the military.

2.2 Cobalt

Cobalt, a transition series metallic element having atomic number 27, is similar to silver in appearance. Cobalt and cobalt compounds have expanded from use colorants in glasses and ground coat fits for pottery to drying agents in paints and lacquers, animal and human nutrients, electroplating materials, and high temperature alloys, hard facing alloys, and high speed tools, and magnetic alloys, alloys used for prosthetics, and used in radiology. Cobalt is also as a catalyst for hydrocarbon refining from crude oil for the synthesis of heating fuel.

The electronic structure of cobalt is $[\text{Ar}]3d^7 4s^2$. At room temperature the crystalline structure of the α (or ϵ) form, is close-packed hexagonal (cph) and lattice parameters are $a = 0.2501$ nm and $c = 0.4066$ nm. Above approximately 417°C , a face-centered cubic (fcc) allotrope, the γ (or β) form, having a lattice parameter $a = 0.3554$ nm, becomes the stable crystalline form. The scale formed on unalloyed cobalt during exposure to air or oxygen at high temperature is double-layered. In the range of 300 to 900°C , the scale consists of a thin layer of mixed cobalt oxide, Co_3O_4 , on the outside and cobalt (II) oxide, CoO , layer next to metal. Cobalt (III) oxide, Co_2O_3 , may be formed at temperatures below 300°C . Above 900°C , Co_3O_4 decomposes and both layers,

although of different appearance, are composed of CoO only. Scales formed below 600°C and above 750°C appear to be stable to cracking on cooling, whereas those produced at 600-750°C crack and flake off the surface.

Cobalt forms numerous compounds and complexes of industrial importance. Cobalt, atomic weight 58.933, is one of the first transition series of Group 9 (VIII B). There are thirteen known isotopes, but only three are significant: ^{59}Co is the only stable and naturally occurring isotope; ^{60}Co has a half-life of 5.3 years and is a common source of γ -source for Mössbauer spectroscopy. Cobalt exists in the +2 or +3 valence states for the major of its compounds and complexes. A multitude of complexes of the cobalt (III) ion exists, but few stable simple salt are known. Octahedral stereochemistry is the most common for cobalt (II) ion as well as for cobalt (III). Cobalt (II) forms numerous simple compounds and complexes, most of which are octahedral or tetrahedral in nature; cobalt (II) forms more tetrahedral complex than other transition-metal ions. Because of the small stability difference between octahedral and tetrahedral complexes of cobalt (II), both can be found in equilibrium for a number of complexes. Typically, octahedral cobalt (II) salts and complexes are pink to brownish red; most of the tetrahedral Co (II) species are blue.

Table 2.1 Physical properties of cobalt (Othmer, 1991)

Property	Value
atomic number	27
atomic weight	58.93
transformation temperature, °C	417
heat of transformation, J/g ^a	251
melting point, °C	1493
latent heat of fusion, ΔH_{fus} J/g ^a	395
boiling point, °C	3100
latent heat of vaporization at bp, ΔH_{vap} kJ/g ^a	6276
specific heat, J/(g °C) ^a	
15-100°C	0.442
molten metal	0.560

coefficient of thermalexpansion, °C ⁻¹			
cph at room temperature		12.5	
fcc at 417 °C		14.2	
thermal conductivity at 25 °C, W/(m·K)		69.16	
thermal neutron absorption, Bohr atom		34.8	
resistivity, at 20 °C ^b , 10 ⁻⁸ Ω·m		6.24	
Curie temperature, °C		1121	
saturation induction, 4πI _s , T ^c		1.870	
permeability, μ			
initial		68	
max		245	
residual induction, T ^c		0.490	
coercive force, A/m		708	
Young's modulus, Gpac		211	
Poisson's ratio		0.32	
Hardness ^f , diamond pyramid, of %Co		99.9	99.98 ^e
At 20 °C		225	253
At 300 °C		141	145
At 600 °C		62	43
At 900 °C		22	17
strength of 99.99 %cobalt, MPa ^g	as cast	annealed	sintered
tensile	237	588	679
tensile yield	138	193	302
compressive	841	808	
compressive yield	291	387	

^a To convert J to cal, divided by 4.184.

^b conductivity = 27.6 % of International Annealed Copper Standard.

^c To convert T to gauss, multiply by 10⁴.

^d To convert GPa to psi , multiply by 145,000.

^e Zone refined.

^f Vickers, ^g To convert MPa to psi , multiply by 145.

2.3 Cobalt(II, III) Oxides

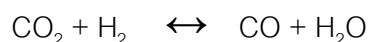
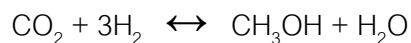
Cobalt has three well-known oxides: Cobalt (II) oxide, CoO , is an olive green, cubic crystalline material. Cobalt (II) oxide is the final product formed when the carbonate or the other oxides are calcined to a sufficiently high temperature, preferably in a neutral or slightly reducing atmosphere. Pure cobalt (II) oxide is a difficult substance to prepare, since it readily takes up oxygen even at room temperature to re-form a higher oxide. Above about $850\text{ }^{\circ}\text{C}$, cobalt (II) oxide form is the stable oxide. The product of commerce is usually dark gray and contains 77-78 wt% cobalt. Cobalt (II) oxide is soluble in water, ammonia solution, and organic solvents, but dissolves in strong mineral acids. It is used in glass decorating and coloring and is a precursor for the production of cobalt chemical.

Cobalt (III) oxide, Co_2O_3 , is formed when cobalt compounds are heated at a low temperature in the presence of an excess of air. Some authorities hold that cobalt (III) oxide exists only in the hydrate form. The lower hydrate may be made as a black powder by oxidizing neutral cobalt solutions with substances like sodium hypochlorite. Co_2O_3 or $\text{Co}_2\text{O}_3 \cdot \text{H}_2\text{O}$ is completely converted to Co_3O_4 at temperatures above $265\text{ }^{\circ}\text{C}$. Co_3O_4 will absorb oxygen in a sufficient quantity to correspond to the higher oxide Co_2O_3 .

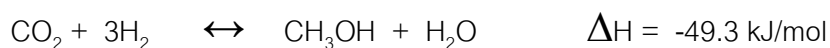
Cobalt oxide, Co_3O_4 , is formed when cobalt compounds, such as the carbonate or the hydrated sesquioxide, are heated in air at temperatures above approximately $265\text{ }^{\circ}\text{C}$ and not exceeding $800\text{ }^{\circ}\text{C}$.

2.4 CO_2 Hydrogenation Reactions

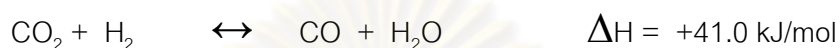
In recently, several reaction mechanisms for the CO_2 hydrogenation have been proposed. First, the catalytic hydrogenation over promoted Cu-ZnO catalysts under pressurized conditions produces mainly CH_3OH , CO and H_2O . A small amount of CH_4 was produced. At higher temperature, a very small amount of CH_3OCH_3 was also produced. Therefore, the main reactions are shown in the following equations (Arakawa et al., 1992).



However, there are reactions of methanol synthesis from CO_2 , showed in following equations. Methanol synthesis from CO_2 :



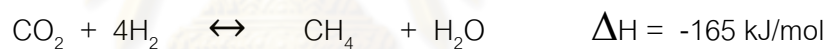
Reverse water gas shift :



Methanol synthesis from CO :



Furthermore, Lahtinen et al., (1994) proposed the reaction mechanisms for C, CO and CO_2 hydrogenation shown in figure 3.5. Moreover, CO and CO_2 methanation is investigated as an alternative purification step (Choudhury, 2006; Xu, 2006; Dagle, 2007)



ศูนย์วิทยทรัพยากร
จุฬาลงกรณ์มหาวิทยาลัย

CHAPTER III

LITERATURE REVIEW

3.1 Activated carbon from other precursors

As is well known, the activated carbon prepared from different precursors or prepared by different activation process, will have different textural characteristics that are shown in **table3.1**. Furthermore, it was usually applied as potential adsorbents for the purification of gases (Guo, 2002; Azevedo, 2007), for the removal of organic pollutants from water (Zhou et al., 2009), and etc.

Table 3.1 Comparisons of the characteristics of porosity of other literature data for other precursors under optimum condition

References	Precursor	Activation method	S _{BET} (m ² /g)	V _{tot} (cm ³ /g)	V _{micro} (cm ³ /g)
Guo et al.,2002	Rice husk	Chemical(KOH)	more than 3,000	1.9	
Wei et al.,2006	Coconut shell	Physical(Air)	more than 700		
Azevedo et al.,2007	Coconut shell	Chemical activation with ZnCl ₂ followed by physical activation	2,114	1.307	1.142
Li et al.,2008	Coconut shell	Physical(stream)	1,926	1.26	0.931
Kalderis et al.,2008	Rice husk	Chemical(ZnCl ₂)	750	0.38	
Basta et al.,2009	Rice straw	Chemical(KOH)	1,917	0.94	
Guo et al.,2009	Coconut shell	Physical(CO ₂)	1,700	1.135	0.882
Liou and Wu, 2009	Rice husk	Chemical(ZnCl ₂)	2,434	1.344	

3.2 Activated carbon from rice bran

There have reported that few researchers used rice bran as precursor for activated carbons. Suzuki et al. (2007) reported the preparation of activated carbons from deoil rice brans by using pre-carbonization with H_2SO_4 and then physical activation(CO_2) as activation method that resulted in a BET surface area of $625 \text{ m}^2/\text{g}$ and a pore volume of $0.137 \text{ cm}^3/\text{g}$ (mesopores predominance). These results indicated that rice bran could be an economically promising material. Meanwhile, Kumar et al. (2009) prepared activated carbons from rice brans by using pre-carbonization followed by chemical activation (H_3PO_4) as activation method that resulted in a BET surface area of $794 \text{ m}^2/\text{g}$ and a pore volume of $0.43 \text{ cm}^3/\text{g}$. This was used as carrier matrix for immobilization of acid protease. In addition, activated carbon from rice bran was applicable as carrier matrix for immobilization of a mutant strain of *Pseudomonaspictorum* (MU 174) (Chitra et al., 1996).

3.3 Co catalyst

In many years later, cobalt is the metal which was proposed by Fischer and Tropsch as the first catalysts for syngas conversion that has been used as a Fischer – Tropsch catalyst in the industry for hydrocarbon synthesis due to their high activity and high selectivity for linear hydrocarbon, high stability, low water-gas shift activity and lower price compared to noble metal (Sun, 2000; Dutta, 2004). However, cobalt-based catalysts are very sensitive to sulfur, which could readily contaminate them. So the amount of sulfur in the feed should be much less than 0.1 ppm. In addition, they have to operate at a very narrow range of temperatures and pressures. Increasing in temperature leads to a spectacular increase in methane selectivity for Cobalt catalysts used in the low-temperature Fischer – Tropsch process (473-513 K) in synthesis of linear long-chain hydrocarbon waxes and paraffins (Jager, 1998; Espinoza, 1999; Jager, 1995). So, cobalt catalysts represent the optimal choice for synthesis of long-chain hydrocarbons in Fischer – Tropsch process.

There were studies for active sites in cobalt catalyst in many directions, such as unsupported metallic cobalt and cobalt monocrystals were active, for large cobalt metal particles the reaction rate is proportional to the number of cobalt surface sites (Iglesia et al., 2003). In addition, the active cobalt metallic phases, a working FT

catalyst, could contain several other cobalt species: cobalt carbide, cobalt oxides, cobalt support mixed compounds, etc. These species are probably not directly involved in FT synthesis. Cobalt carbide formation be related to a deactivation process that lead to the activity of Fischer-Tropsch reaction over Co-based catalysts decreased. However, some promoters could restrain the formation of cobalt carbide (Xiong et al., 2005). Oxidized cobalt species (Co_3O_4 , CoO , etc.) do not catalyze FT synthesis either. Oxidation of cobalt metallic species during the reaction leads to catalyst deactivation and reduces FT reaction rates. At the same time, cobalt oxidized species could probably affect the rate of several side and secondary reactions, such as water-gas shift, olefin isomerization, reinsertion, and hydrogenolysis (Khodakov, 2007).

Matsuzaki et al. (1996) found that highly dispersed cobalt metal catalysts supported on SiO_2 that prepared by using cobalt(II)acetate as a precursor promoted with noble metals such as Ir, Ru, Rh, Re, Pt or OS in hydrogenation of carbon monoxide were active for the formation of oxygenates by CO hydrogenation and the vapor phase hydroformylation of ethene. The selectivity of oxygenates, especially C_2 -oxygenates, was strongly enhanced by a further modification with basic additives such as alkali and alkaline earth cations. Furthermore, highly dispersed Co^{2+} particles are formed on SiO_2 by the decomposition of Co(II) acetate at an elevated temperature in flowing H_2 and the noble metals promote the reduction of the Co^{2+} particles to cobalt metals by spilt-over hydrogen activated on the noble metal sites that are shown in Figure 3.1 and Figure 3.2, respectively.

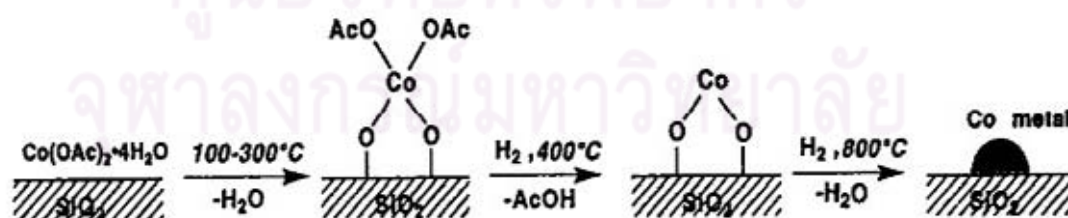


Figure 3.1 Proposed decomposition procedure of Co (II) acetate on SiO_2 . (Matsuzaki et al., 1996)

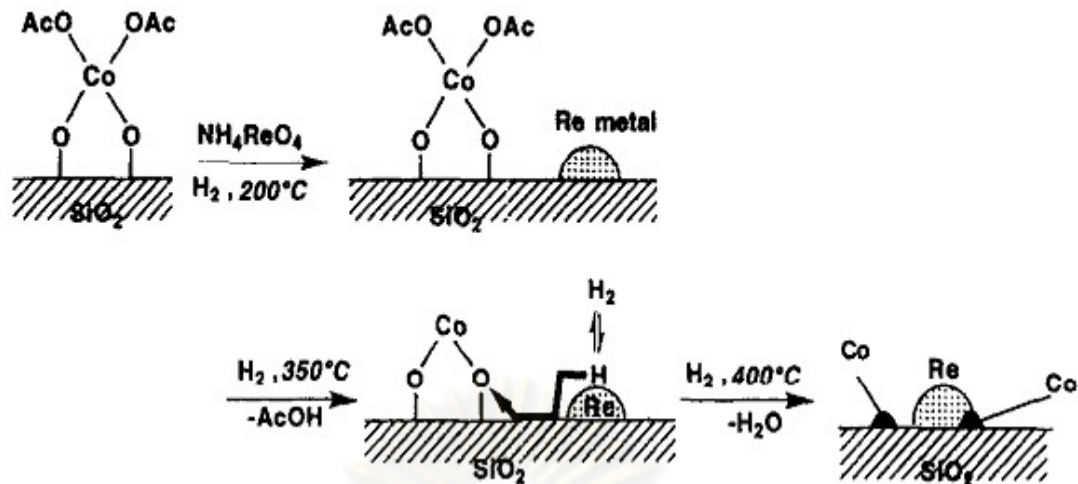


Figure 3.2 Proposed reduction procedure of Co species of Co(II)-Re/SiO₂.
(Matsuzaki et al., 1996)

Meanwhile, Sun et al. (2000) found that catalysts prepared by mixed impregnation of cobalt(II) nitrate and cobalt(II) acetate displayed higher activity than the catalysts prepared from either mono-precursor at mild reaction conditions (1MPa total pressure, H₂/CO= 2, T= 513K) of Fischer–Tropsch synthesis (FTS) and assumed that the metal readily reduced from cobalt nitrate promoted the reduction of Co²⁺ to metallic state in cobalt acetate by H₂ spillover mechanism during catalyst reduction process(Figure 3.3).

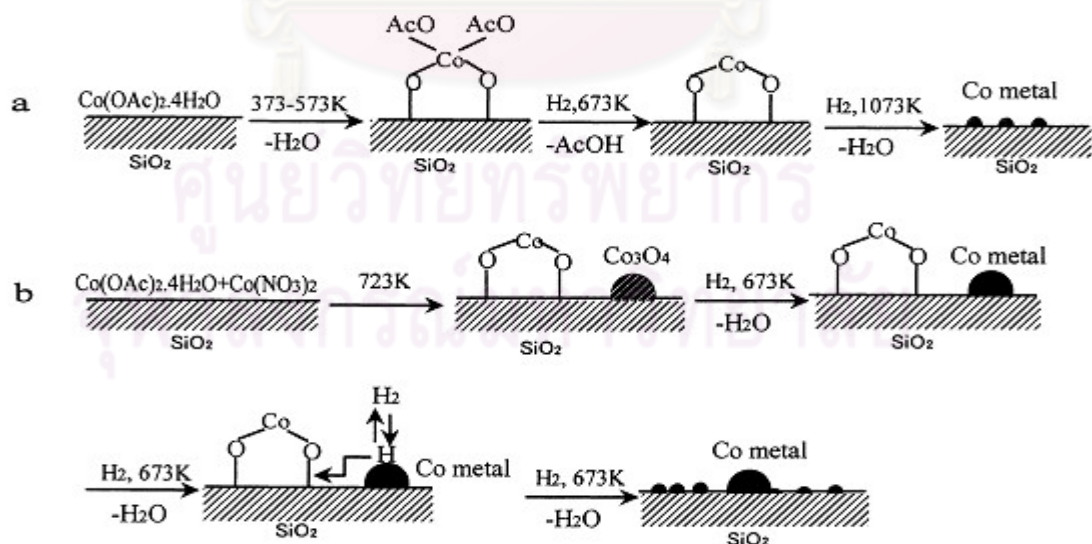


Figure 3.3 Proposal reduction procedure of Co(II)acetate, Co(II)nitrate/Co(II)acetate on silica during catalyst preparation.; a: Co(II)acetate; b: cobalt(II)nitrate/cobalt(II)acetate.
(Sun et al., 2000)

Visconti et al. (2009) found that the hydrogenation of CO and CO₂ on Co/Al₂O₃ Fischer–Tropsch catalyst under low temperature FTS conditions showed a higher CO₂ reactivity with respect to CO. However, the selectivity of the CO and CO₂ hydrogenation process was found to be extremely different: CO hydrogenation leads to a classical FT product distribution, while the products of CO₂ hydrogenation consist mainly of methane (with selectivity near 90%) and light hydrocarbons that result to be similar with report of Zhang et al. (2002).

Dutta et al. (2004) found that 15% Co/SiO₂ catalysts yield higher CO and syngas conversions with higher methane selectivity than 15% Co/ Al₂O₃ catalysts. Conversely the Al₂O₃ supported catalysts gave much higher selectivity towards olefins than Co/SiO₂. These results yield the correlation that the presence of Co₃O₄ yield higher methane selectivity whereas the presence of Co²⁺ species yields lower methane selectivity but higher olefin selectivity.

3.4 CO₂ Hydrogenation Reactions

In a few years ago, efficient heterogeneous catalysts have usually been developed for CO₂ hydrogenation to methanol. However, the thermodynamics for methanol production from H₂ and CO₂ are not as favorable as that for production of methanol from H₂ and CO. For example, at 200°C the equilibrium yield of methanol from CO₂ is slightly less than 40% while the yield from CO is greater than 80% (Arakawa et al., 1998). For methanol synthesis, Fisher and Bell (1997) studied Cu/ZrO₂/SiO₂ catalysts by in-situ infrared spectroscopy and suggested the pathway for the route to methanol that was shown in **Figure 3.4**. Meanwhile, Bando et al. (1997) found that TiO₂-supported Cu catalyst showed the highest TOFs (turn-over frequencies) among Cu/Al₂O₃, Cu/SiO₂, and Cu/TiO₂ for methanol synthesis from CO₂ hydrogenation. In addition, Kusama et al. (2001) found that Rh-Co/SiO₂ catalysts showed methanol formation more than Rh/SiO₂. Whereas, ethanol has also been produced by the hydrogenation of CO₂ (Kusama et al., 1996). This fuel is attractive because it has a somewhat higher energy density than methanol and it is not as toxic. However, the selectivity for ethanol production is generally low (<40%).

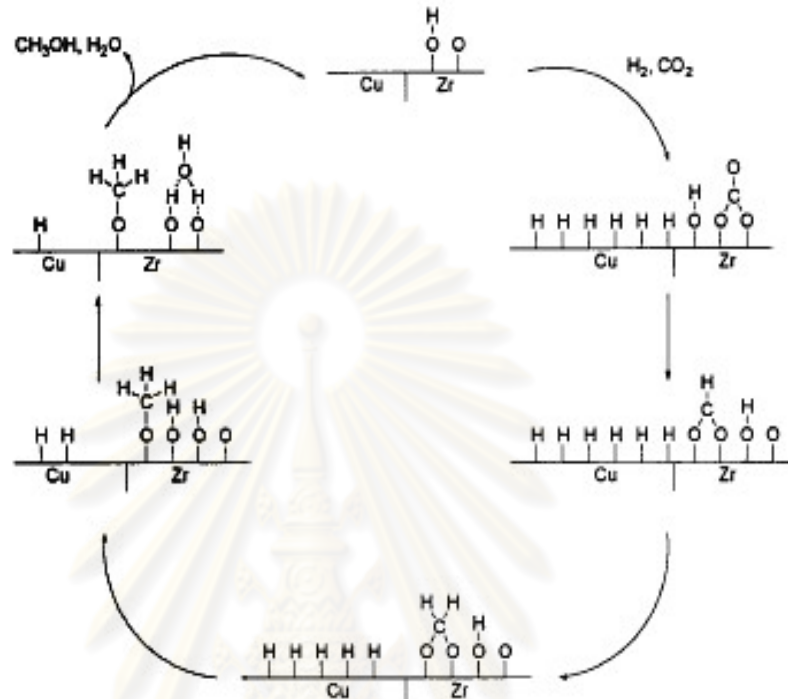


Figure 3.4 Proposed mechanism for the heterogeneous catalytic hydrogenation of CO₂ to methanol. (Fisher and Bell, 1997)

The hydrogenation of CO₂ to methane and higher hydrocarbons is also known that when compared with CO hydrogenation in the same catalysts that was cobalt Fischer-Tropsch synthesis catalysts found that catalytic activities were similar obtained but selectivities were very different. For CO hydrogenation, normal Fischer-Tropsch synthesis product distributions were mostly observed. In contrast, the CO₂ hydrogenation products contained about 70% or more of methane (Zhang et al., 2002) that result to be similar with report of Visconti et al. (2009). In addition, Dorner et al. (2009) reported influence of gas feed composition and pressure on the catalytic conversion of CO₂ to hydrocarbons on a traditional cobalt-based Fischer-Tropsch catalyst (Co-Pt/Al₂O₃) found that reducing the feed gas ratio of H₂/CO₂ from 3:1 to 2:1 and subsequently to 1:1 and lowering the operating pressure has led to the modification of the product distribution toward longer chain HC. Furthermore, Lahtinen et al. (1994)

reported C, CO and CO₂ hydrogenation on cobalt foil model catalysts found that the reactions produce mainly methane but with selectivities of 98, 80, and 99 wt% at 525 K for C, CO, and CO₂, respectively. These authors also proposed the reaction mechanisms for C, CO and CO₂ hydrogenation that were shown in figure 3.5.

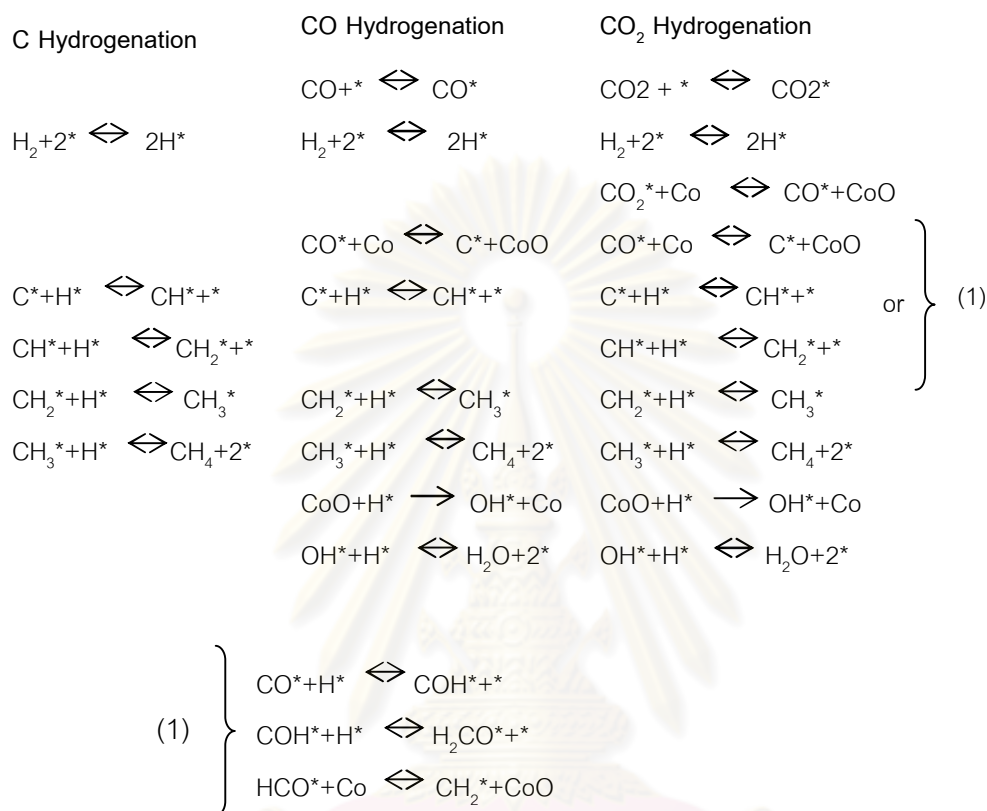


Figure 3.5 The reaction mechanisms proposed for C, CO and CO₂ hydrogenation. In the case of CO₂ hydrogenation two alternative reaction paths are given. The rate limiting step is shown with a one-way arrow (\rightarrow). (Lahtinen et al., 1994)

For the other catalysts in CO₂ hydrogenation, unless a cobalt-based Fischer-Tropsch catalyst. Kowalczyk et al. (2008) found that the catalytic properties of ruthenium surfaces expressed by TOFs (turn-over frequencies) proved to be dependent on the kind of support material and metal dispersion. The following sequence of TOFs was obtained: Ru/Al₂O₃ > Ru/MgAl₂O₄ > Ru/MgO > Ru/C, both CO and CO₂ hydrogenation. Meanwhile, Kusama et al. (2000) reported effect of metal loading on CO₂ hydrogenation reactivity over Rh/SiO₂ catalysts found that the difference in Rh loading significantly changed product selectivity of CO₂ hydrogenation over Rh/SiO₂ catalysts.

The main product was CO for the low loaded catalyst, while CH₄ was dominantly produced on 10 wt.% Rh/SiO₂.

Suo et al. (1997) studied TiO₂-, ZrO₂- and Al₂O₃-supported Fe catalysts for CO₂ hydrogenation found that the catalytic activity was affected by the support used. TiO₂- and ZrO₂- supported iron oxides showed good activity and selectivity in the synthesis of C₂₊ hydrocarbons.

Yamasaki et al. (2006) studied effect of tetragonal ZrO₂ on the catalytic activity of Ni/ZrO₂ catalysts for CO₂ methanation found that the fraction of tetragonal ZrO₂ in the Ni/ZrO₂ catalysts increased with increasing nickel content and the tetragonal zirconia-supported nickel catalysts showed a higher turnover frequency than the monoclinic zirconia-supported nickel catalysts. Meanwhile, Chang et al. (1997) studied Nickel supported on rice husk ash – activity and selectivity in CO₂ methanation found that Nickel catalyst supported on rice husk ash exhibited high activity in methanation of CO₂ and high selectivity (80-90%) for CH₄ formation. Moreover, Lee et al. (2005) studied Raney Ni catalysts for CO and CO₂ methanation activity found that main products were CH₄ and CO₂ in CO methanation, and CH₄ and CO in CO₂ methanation, CO₂ methanation proceeded highly selectively with lower activation energy as compared with CO methanation. The catalyst derived from alloy having higher Ni content using more severe leaching condition showed higher specific activity and higher selectivity to methane in both CO and CO₂ methanation. Increasing specific activity and selectivity can be explained with the higher ability of catalyst to dissociate CO. Thus, in CO and CO₂ methanation on Raney Ni catalyst, catalytic activity seem likely to have close relation with the activity to dissociate CO.

The reverse water gas shift (RWGS) reaction is a part of CO₂ hydrogenation. So, studying the reverse water gas shift (RWGS) reaction is important for studying CO₂ hydrogenation. Chen et al. (2003) studied the reverse water gas shift (RWGS) reaction over with and without potassium promoter Cu/SiO₂ catalyst found that after addition of even a little amount of potassium, Cu/K₂O/SiO₂ obviously offered better catalytic activity than Cu/SiO₂. The coverage of formate species increases on Cu/K catalyst and new active sites could be created at interface between Cu and K. The main role of K₂O was to provide catalytic activity for decomposition of formates, besides

acting as a promoter for CO_2 adsorption. A new reaction mechanism was shown in Figure 3.6. Hydrogen was dissociatively adsorbed on Cu and could spill over to K_2O to associate with CO_2 . This resulted in the formation of formate species for the production of CO.

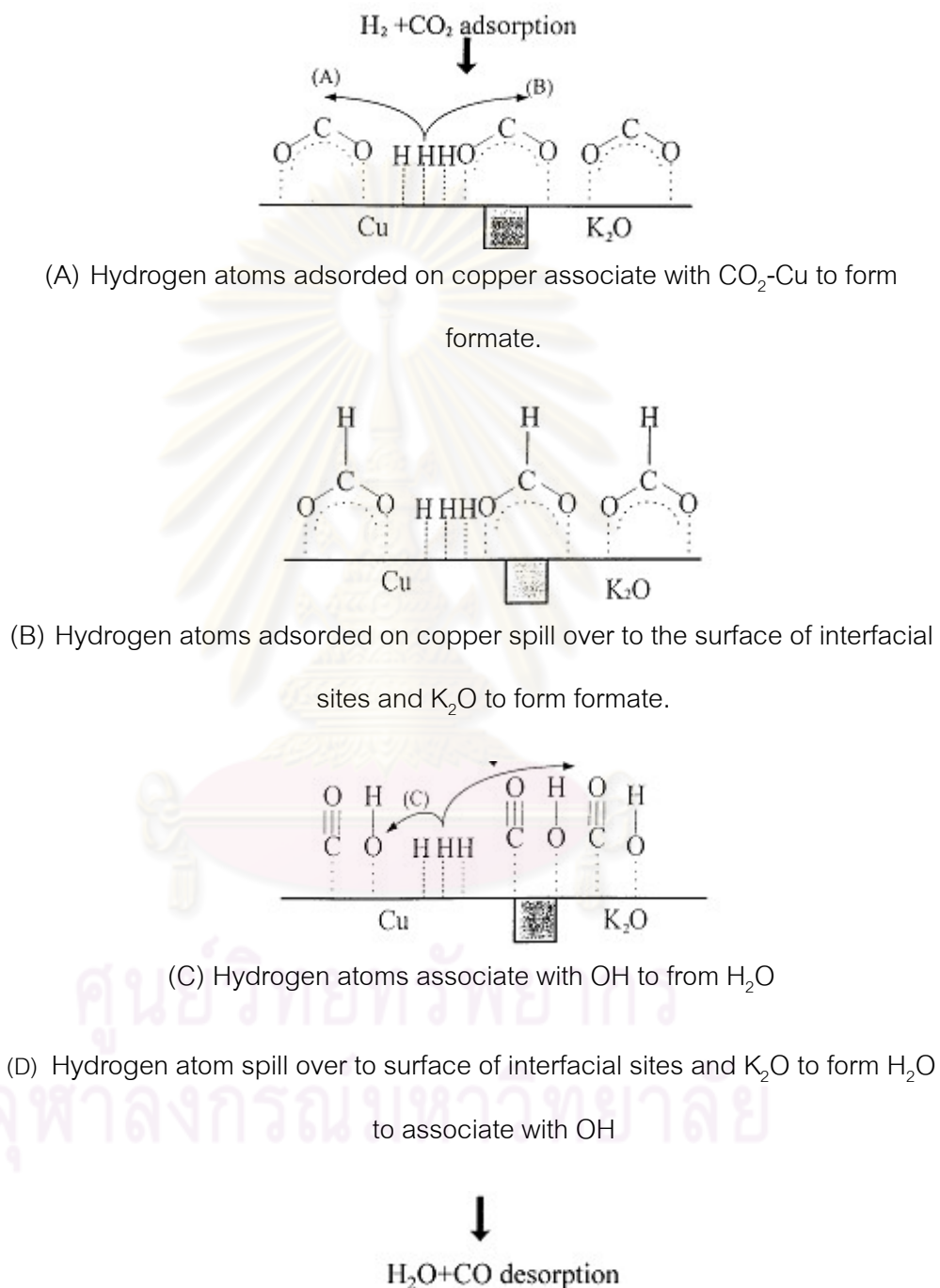


Figure 3.6 Proposed mechanism of CO formation from CO_2 and H_2 on Cu/K/SiO₂ catalyst. (Chen et al., 2003)

Furthermore, Luhui et al. (2008) studied reverse water gas shift reaction over Co-precipitated Ni-CeO₂ catalysts found that 2wt.%Ni-CeO₂ showed excellent catalytic performance in term of activity, selectivity, and stability for RWGS reaction.

3.5 Co/AC catalysts

Activated carbon supported cobalt catalysts were studied by many researcher in several reactions. In Fischer–Tropsch (FT) synthesis, Castilla and Marin (1995) reported the preparation of Co catalysts supported on two different activated carbons obtained from olive stones that the supported catalysts were prepared from Co₂(CO)₈ following either a sublimation or an evaporation technique or from cobalt nitrate following an impregnation technique found that the Co/activated carbon catalysts were structure-insensitive in both H₂/CO and H₂/CO₂ reactions within the dispersion range studied (5-32%). These results indicated that the Co particles were well reduced as a consequence of the low metal-support interactions. In the case of the H₂/CO reaction the selectivity for hydrocarbons production depended on the mean particle size of the catalyst and methane was the main product obtained. In the case of the H₂/CO₂ reaction, methane and CO were the only products detected and the selectivity for methane production decreased with increasing mean particle size of the Co catalyst. At different operating conditions, Zaman et al. (2009) investigated performance of cobalt on Carbon nanotubes (CNTs), Carbon nanotubes grown on MgO (CNTs-MgO), Carbon nanotubes grown on alumina (CNTs-alumina) and activated carbon (AC) found that the cobalt supported on CNTs grown on MgO (Co/CNT–MgO) shows the highest selectivity to C₅₊ as the most desired FTS products. The C₅₊ selectivity enhancement was about 37, 34, 17, and 77% as compared to the Co/CNT, Co/alumina, Co/CNTs-alumina, and Co/activated carbon, respectively. In addition, Co/AC shows a BET surface area of 927 m² while the other catalysts show moderate BET areas in the range of 17–96 m²/g, and Co/AC shows highest CH₄ and lowest C₅₊ selectivity, possibly due to high BET surface area, diffusion limitations, and small cobalt crystallite sizes on activated carbon. Ma et al. (2004) reported effect of Co Loading and Promoters (K, Ce, Zr) on activated carbon supported in Fischer-Tropsch synthesis found that Co loading affected initial syngas conversion and CH₄ selectivity in the following order : 20%Co > 15%Co > 10%Co > 7%Co, the unpromoted Co/AC catalysts (7-20%Co) showed 25.9-73.1% initial syngas

conversion and 1.3-2.4% CO₂ selectivity. In case of K, Ce, and Zr promoters would remarkably change the initial catalytic performance of the Co/AC catalysts, addition of K into the Co/AC catalyst significantly decreased the FTS activity and CH₄ selectivity but increased the water gas shift (WGS) activity, addition of Ce improved the Co/AC catalyst activity and high CH₄ selectivity, addition of Zr increased the FTS activity. Moreover, K, Ce and Zr promoters improved Co dispersion and interaction between Co oxide and the AC surface which might be the reasons for the subsequent catalyst performance, especially for the Ce- and Zr-promoted catalysts. Furthermore, vanadium (V) promoter affected on activated carbon supported cobalt catalysts in Fischer–Tropsch synthesis. It was found that the CO conversion could be significantly increased from 38.9 to 87.4% when 4 wt.% V was added into Co/AC catalyst. Small amount of vanadium promoter could improve the selectivity toward C₁₀–C₂₀ fraction and suppress the formation of light hydrocarbon. However, excess of vanadium increased methane selectivity and decreased C₊₅ selectivity (Wang et al., 2006). Wang et al. (2008) reported CO conversion increased from 86.4% to 92.3% and the selectivity to methane decreased from 14.2% to 11.5% and C₅₊ selectivity increased from 71.0% to 74.7% when low La loading (La = 0.2wt%) was added into the Zr-Co/AC catalyst. However, high loadings of La (La = 0.3-1.0 wt%) decreased catalyst activity as well as the C₅₊ selectivity and increased methane selectivity. Moreover, Xiong et al. (2005) reported formation of Co₂C species in activated carbon supported cobalt-based catalysts and its impact on Fischer–Tropsch reaction found that the cobalt carbide (Co₂C) species was formed in some activated carbon supported cobalt-based (Co/AC) catalysts during the activation of catalysts and the activity of Fischer–Tropsch reaction over Co-based catalysts decreased due to the formation of these cobalt carbide species. However, some promoters and pretreatment of activated carbon with steam could restrain the formation of cobalt carbide.

Lu et al. (2009) reported cobalt catalyst supported on porous carbons derived from rice husk and carbon nanotube for treating of gas pollutants. That porous carbons were prepared from rice husks, commercial coconut-shell-derived carbon, and carbon nanotube (CNT) by activation with CO₂, KOH, and ZnCl₂. Cobalt catalysts were supported on the six different porous carbons by excess-solution impregnation and

were used to carry out reactions with different constituents, such as NO + CO, toluene, NO + toluene, and NO + CO + toluene. It was found that the cobalt catalysts supported on rice-husk-based carbon activated by CO₂ and those on commercial-activated-carbon retreated by KOH showed 100% conversion on toluene oxidation. Among the six porous supported catalysts, the cobalt catalysts prepared with CNT and rice-husk-derived carbon by using CO₂ showed the best catalytic activity and thermal stability when compared to the others. In addition, Lu et al. (2007) reported preparation the activated carbons supported transition-metal catalyst by the polyol method for VOC oxidation that copper, cobalt, iron, and nickel were used as the catalytic active phases. It was found that the catalysts prepared by the polyol process exhibited well-dispersed nanoscale metal particles. Increasing in the reduction time and the particle size led to a lower toluene conversion. The activity of metal/AC with respect to metal was observed to follow a particular order: Cu > Co > Fe > Ni. Increasing the reaction temperature and decreasing the toluene concentration and space velocity resulted in better VOC conversion.

Faria et al. (2009) reported metal oxides (cerium, manganese and cobalt oxides) supported on activated carbon for the removal of selected organic compounds. It was found that metal oxides supported on activated carbon have been shown to be effective ozonation catalyst for the degradation of aromatic compounds (sulfanilic acid and aniline) and an azo textile dye. Nevertheless, when comparing the respective results with those obtained with the commercial activated carbon, it should be noticed that a significant part of the catalytic effect observed must be attributed to the support.

Xu et al. (2008) reported hydrogen production from alkaline sodium borohydride (NaBH₄) solution via hydrolysis process over activated carbon (activated carbons are used in their original form and after liquid phase oxidation with HNO₃) supported cobalt catalysts. It was found that the oxidative treatment led to the formation of various functional groups on the surface of the activated carbon and cobalt catalysts supported on the modified activated carbon exhibited higher activity and stability.

Lu and Wey (2007) found that Co/CNT generated about 99% of the high activity for CO conversion at 250°C and thermally stability that is superior to Co/activated carbon for CO oxidation at low temperature.

Pilecka et al. (2006) reported cobalt, iron and Co-Fe catalysts on activated carbon in ammonia synthesis and barium or potassium were used as promoters. It was found that the average sizes of crystallites (20–30 nm) were roughly independent of the metal kind (Co, Fe, Co-Fe). The effects of Ba and K on the catalyst performance proved to be strongly dependent on the choice of an active phase (Co or Fe or Co-Fe). In the case of Co/C, the promotional effect of barium was extremely large. Furthermore, the Ba-Co/C system was found to be less inhibited by the ammonia product than Ba-Fe/C. At low temperature (400°C) and at high conversion (8% NH₃ in the gas), the surface-based reaction rate (TOF) for Ba-Co/C was about six times higher than that for Ba-Fe/C.

Zhu et al. (1999) reported catalytic conversion of N₂O to N₂ over Co/AC and Cu/AC Catalysts. It was found that Increasing loading of Co or Cu led to decreasing dispersion, but 20 wt % loading was an upper limit for optimal activities in both cases, with too high loading causing sintering of metal. Co exhibited a relatively better dispersion than Cu. Impregnation of metal led to a large decrease in surface area and pore volume, especially for 30 wt % of loading. 20 wt % of loading has proved to be the optimum for both Cu and Co, which showed the highest activity.

Jiao et al. (2009) reported effect of La₂O₃ doping on syntheses of C₁–C₁₈ mixed linear α -alcohols from syngas over the Co/AC catalysts. The results showed that the selectivity towards alcohols was improved by doping La into the 15Co/AC catalysts and the reducibility of the 15Co-xLa/AC catalyst decreased and the Co dispersion improved due to the strong interaction between Co and La₂O₃ species. La₂O₃ could promote the formation of cobalt carbides (Co₂C) which are postulated to play an important role in the syntheses of the mixed linear α -alcohols. On the other hand, high Co dispersion and an appropriate ratio of Co²⁺/Co⁰ could enhance the activity of CO hydrogenation.

CHAPTER IV

EXPERIMENTAL

4.1 Preparation activated carbon

4.1.1 Chemical

1. Sulphuric acid (H_2SO_4)
2. Sodium bicarbonate (NaHCO_3)
3. Zinc chloride (ZnCl_2)
4. Phosphoric acid (H_3PO_4)
5. Hydrochloric acid (HCl)
6. Distilled water

4.1.2 Experimental procedure

1. The deoil rice bran (RB) was treated with concentrated sulphuric acid (weight ratio 1:1) for 24 hours at 150°C . Then, the sample was cooled.
2. The resulting material was ground.
3. The excess of the acid present on the material was leached out by washing with a sodium bicarbonate solution (1%w/v) until neutrality and was several washed with distill water. Then, the sample was dried at 110°C for 24 hours.
4. The treated material was impregnated with H_3PO_4 or ZnCl_2 at 1:1 by w/w and then was dried at 110°C for 24 hours.
5. The impregnated material was activated under a nitrogen gas flow at 200 ml/min and at the desired temperature (400, 500, 600, 700°C) with a heating rate $10^\circ\text{C}/\text{min}$. Once the activation temperature was reached, it was kept for 1 hour before cooling the furnace down to room temperature.
6. The activated material was stired in 1 M HCl solution at 70°C for 6 hours.

7. The resulting materials were washed with distilled water several times until neutrality to remove residual chemicals.
8. The washed sample was dried at 110°C for 24 hours to be as activated carbon.

4.2 Cobalt Loading

4.2.1 Chemical

1. Cobalt(II)nitrate hexahydrate 98+% [Co(NO₃)₂·6H₂O] available from Aldrich.
2. De-ionized water

4.2.2 Experimental procedure

In this experiment, incipient wetness impregnation is the one methods used for loading cobalt. Cobalt (II) nitrate hexahydrate [Co(NO₃)₂·6H₂O] was used as precursor in this method.

The incipient wetness impregnation procedure is as follow:

1. The certain amount of cobalt (20 wt% loading) was introduced into the de-ionized water which its volume equals to pore volume of catalyst.
2. The aqueous solution of cobalt was slowly impregnated to Activated carbons.
3. The catalyst was dried in the oven at 110°C for 24 h.
4. The catalyst was calcined in N₂ at 350°C for 6 h.

4.3 Catalyst Nomenclature

Part I: Preparation of activated carbon

Nomenclature of sample is given as follows AC_X_Y

where X is activating agent that here is ZnCl₂ or H₃PO₄.

Y is activation temperature in °C

i.e. AC_ZnCl₂_400 means activated carbon obtained using ZnCl₂ as activating agent and activation temperature at 400°C.

Part II: Catalyst for CO₂ hydrogenation

Nomenclature of sample is given as follows Co/AC_X_Y

Where Co is 20%wt of cobalt impregnated

AC_X_Y is a symbol of activated carbon that was explained above.

i.e. Co/AC_ZnCl₂_400 means activated carbon, obtained using ZnCl₂ as activating agent and activation temperature at 400°C, which impregnated with 20%wt Co.

4.4 Catalyst Characterization

4.4.1 Proximate analysis(ASTM D3173-D3175)

Moisture content determination (ASTM D3173)

The moisture content of materials was determined by ASTM D3173 on oven-drying the material at 110°C until consistency of weight was obtained.

Ash content determination (ASTM D3174)

The total ash content of the materials was determined using crucibles containing dried deoil rice bran heated in a muffle furnace at 750°C based on the procedure by ASTM 3174. After heating, the crucibles were allowed to cool in desiccators and weighed. The residue weight was calculated and reported as percentage of ash by

$$\%ash = \left(\frac{\text{remaining weight(g)}}{\text{original material weight(g)}} \times 100 \right) \quad \dots (4.1)$$

Volatile matter determination (ASTM D3175)

The volatile matter was determined using crucibles containing dried deoil rice bran heated in a muffle furnace at 950°C for 6 minutes based on the procedure by ASTM 3175. After heating, the crucibles were allowed to cool in a desiccators and weighed. The residue weight was calculated and reported as percentage of volatile matter by

$$\%volatile\ matter = \left(\frac{\text{original material weight(g)} - \text{remaining weight(g)}}{\text{original material weight(g)}} \times 100 \right) - \text{Moisture content} \dots (4.2)$$

4.4.2 Elemental analyzer

At least 0.3 mg of deoil rice bran was studied C, H, N composition that analyze by elemental analyzer or CHNS/O analyzer with perkin elmer, PE2400 series II. The sample was decomposed to gas phase by pyrolysis in high-purity oxygen and then

gaseous products were chromatographically separated by frontal analysis with quantitatively detected by thermal conductivity detector (TCD).

4.4.3 X-ray diffraction (XRD)

XRD was performed to determine the bulk phase of catalysts by SIEMENS D 5000 X-ray diffractometer using $\text{CuK}\alpha$ radiation with Ni filter in the 2θ range of 10-80 degrees resolution 0.04° . The crystallite size was calculated from Scherrer's equation.

4.4.4 N_2 Physisorption

The catalyst 50 mg was study BET surface area, pore volume and pore diameter were measured by N_2 adsorption-desorption isotherm at liquid nitrogen temperature (-196°C) using a Micromeritics ASAP 2020. The surface area and pore distribution were calculated according to Brunauer-Emmett-Teller (BET) and Horvath-Kawazoe (H-K) methods, consecutively.

4.4.5 CO Chemisorptions

The active sites and the relative percentages dispersion of cobalt catalyst were determined by CO chemisorptions technique using Micromeritics ChemiSorb 2750 and ASAP 2101C V.3.00 software. It was carried out using 50 mg of a sample and reduced in H_2 flow rate at 50 ml/min with heated from room temperature to 400°C at rate $10^\circ\text{C}/\text{min}$ and held at this temperature for 3 h after the cooled down to room temperature in a He flow. Desorbed CO was measured using thermal conductivity detector. Pulsing was continued until no further carbon monoxide adsorption was observed. Amount of carbon monoxide adsorption on catalyst was relative amount of active site.

4.4.6 Temperature-programmed reduction (TPR)

TPR was used to determine the reducibility of catalysts. The catalyst sample 50 mg was used in the operation and temperature ramping from 35°C to 800°C at $10^\circ\text{C}/\text{min}$. The carrier gas is be 5 % H_2 in Ar. During reduction, a cold trap was placed to before the detector to remove water produced. A thermal conductivity detector (TCD) was measured the amount of hydrogen consumption. The calibration of hydrogen consumption was performed with bulk cobalt oxide at the same conditions.

4.4.7 X-ray photoelectron spectroscopy (XPS)

The XPS analysis was performed originally using an AMICUS spectrometer equipped with a Mg Ka X-ray radiation. For a typical analysis, the source was operated

at voltage of 15 kV and current of 12 mA. The pressure in the analysis chamber was less than 10^{-5} Pa. The AMICUS system is computer controlled using the AMICUS "VISION 2" software.

4.4.8 Transmission Electron Microscopy (TEM)

The morphology and size of the catalyst was observed using JEOL JEM 2010, operating at 200 kV.

4.4.9 Thermal Gravimetric Analysis (TGA)

Thermal gravimetric analysis (TGA) and differential thermal analysis (DTA) were performed using an SDT Analyzer Model Q600 from TA Instruments, USA. The TGA/DTA analyses of the catalysts were carried out from room temperature to 1000 °C at a heating rate of 10 °C/min in N₂.

4.4.10 Scanning Electron Microscopy: SEM and Energy Dispersive X-ray Spectroscopy (EDX)

Scanning electron microscopy (SEM) and Energy dispersive X-ray spectroscopy (EDX) was used to determine the morphology and elemental distribution of the catalyst particles. Model of SEM: JEOL mode JSM-5800LV and EDX was performed using Link Isis Series 300 program at the Scientific and Technological Research Equipment Center, Chulalongkorn University (STREC).

4.4.11 X-ray fluorescence spectrometry (XRF)

X-ray fluorescence spectrometry (XRF) was used to determine the impurity of activated carbons that occurred from synthesis of activated carbons. Amount of element was calculated by theoretical formulas, "fundamental parameter calculation". Model of XRF: Philips model PW2400. at the Scientific and Technological Research Equipment Center, Chulalongkorn University (STREC).

4.4.12 Inductive Coupled Plasma Optical Emission Spectrometer (ICP-OES)

The actual amount of the metals loading were determined by a Perkin Elmer Optima 2100DV AS93 PLUS inductive coupled plasma optical emission spectrometer. The catalysts were prepared in a solution containing 65% HNO₃, 49% HF and 37% HCl with volume ratio 1:3:1 and then filter carbon out.

4.5 Reaction study in CO₂ hydrogenation

4.5.1 Materials

CO₂ hydrogenation was performed using 0.1 g of catalyst packed in the middle of the stainless steel microreactor, which is located in the electrical furnace. The total flow rate is 30 ml/min with the H₂/CO₂ ratio of 10/1. The catalyst sample was reduced *in situ* in flowing H₂ at 400°C for 3 h prior to CO₂ hydrogenation. CO₂ hydrogenation was carried out at 270°C and 1 atm total pressure.

4.5.2 Apparatus

Flow diagram of CO₂ hydrogenation system is shown in Figure 4.1. The system consists of a reactor, an automatic temperature controller, an electrical furnace and a gas controlling system.

4.5.2.1 Reactor

The reactor was made from a stainless steel tube (O.D. 3/8"). Two sampling points were provided above and below the catalyst bed. Catalyst was placed between two quartz wool layers.

4.5.2.2 Automation Temperature Controller

This unit consisted of a magnetic switch connected to a variable voltage transformer and a solid-state relay temperature controller model no. SS2425DZ connected to a thermocouple. Reactor temperature was measured at the bottom of the catalyst bed in the reactor. The temperature control set point is adjustable within the range of 0-800°C at the maximum voltage output of 220 volt.

4.5.2.3 Electrical Furnace

The furnace supplied heat to the reactor for CO₂ hydrogenation. The reactor could be operated from temperature up to 800 °C at the maximum voltage of 220 volt.

4.5.2.4 Gas Controlling System

Reactant for the system was each equipped with a pressure regulator and an on-off valve and the gas flow rates were adjusted by using metering valves.

4.5.2.5 Gas Chromatography

The composition of hydrocarbons in the product stream was analyzed by a Shimadzu GC14B (VZ10) gas chromatograph equipped with a flame ionization detector. A Shimadzu GC8A (molecular sieve 5A) gas chromatography equipped with a thermal

conductivity detector was used to analyze CO and H₂ in the feed and product streams. The operating conditions for each instrument are shown in the Table 4.1.

Table 4.1 Operating condition for gas chromatograph

Gas Chromatograph	SHIMADZU GC-8A	SHIMADZU GC-14B
Detector	TCD	FID
Column	Porapak Q	VZ10
- Column material	SUS	-
- Length	2 m	-
- Outer diameter	4 mm	-
- Inner diameter	3 mm	-
- Mesh range	60/80	60/80
- Maximum temperature	350 °C	80 °C
Carrier gas	He (99.999%)	H ₂ (99.999%)
Carrier gas flow	40 cc/min	-
Column gas	He (99.999%)	Air, H ₂
Column gas flow	40 cc/min	-
Column temperature		
- initial (°C)	60	70
- final (°C)	60	70
Injector temperature (°C)	100	100
Detector temperature (°C)	100	150
Current (mA)	80	-
Analysed gas	Ar, CO ₂ , CO	Hydrocarbon C ₁ -C ₄

4.5.3 Procedures

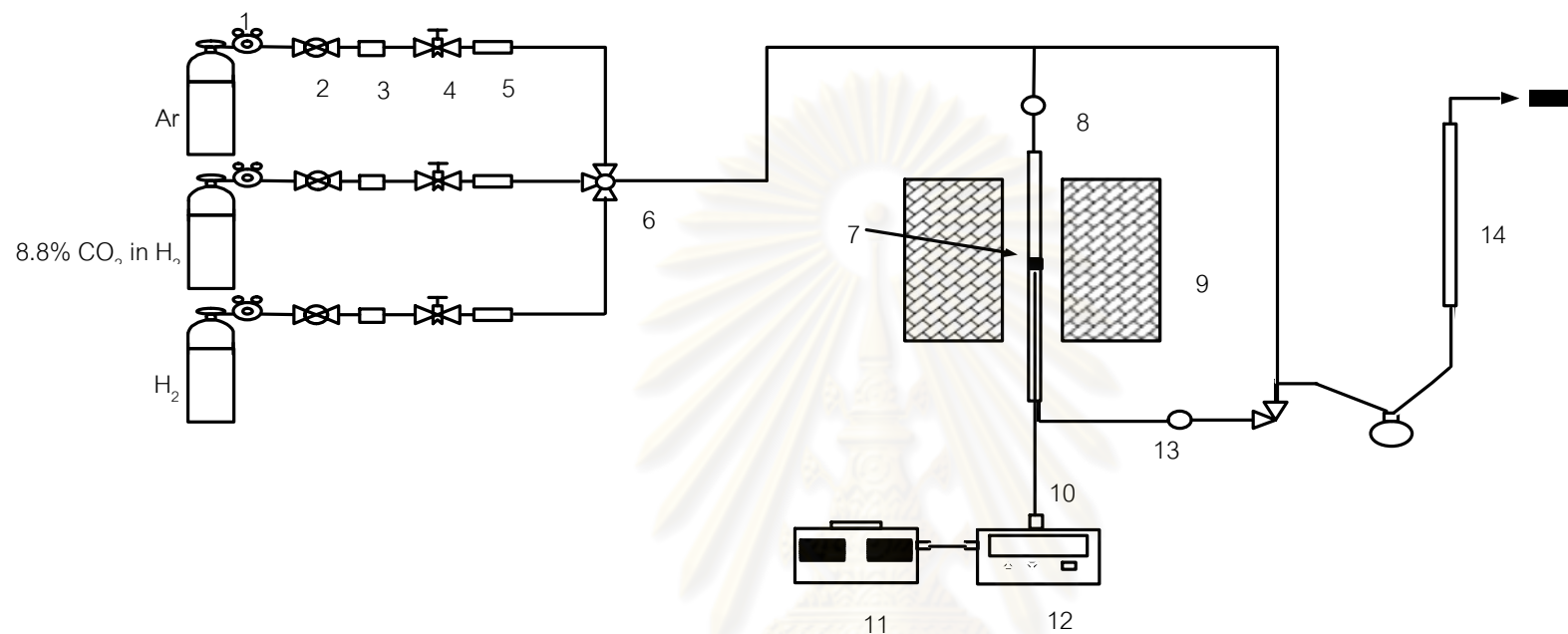
1. Using 0.1 g of catalyst packed in the middle of the stainless steel microreactor, which is located in the electrical furnace.

2. A flow rate of Ar = 8 CC/min, 8.80% CO₂ in H₂ = 22 CC/min and H₂ = 50 CC/min in a fixed-bed flow reactor. A relatively high H₂/CO ratio was used to minimize deactivation due to carbon deposition during reaction.

3. The catalyst sample was reduced *in situ* in flowing H₂ at 400 °C for 3 h prior to CO₂ hydrogenation.

4. CO₂ hydrogenation was carried out at 270 °C and 1 atm total pressure in flowing 8.80% CO₂ in H₂.

5. The effluent was analyzed using gas chromatography technique. [Thermal conductivity detector (TDC) was used for separation of carbon monoxide (CO) and methane (CH₄) and flame ionization detector (FID) were used for separation of light hydrocarbon such as methane (CH₄), ethane (C₂H₆), propane (C₃H₈), etc. In all cases, steady-state was reached within 6 h.



1. Pressure Regulator

2. On-Off Valve

3. Gas Filter

4. Metering Valve

5. Back Pressure

6. 3-way Valve

7. Catalyst Bed

8. Sampling point

9. Furnace

10. Thermocouple

11. Variable Voltage Transformer

12. Temperature Controller

13. Heating Line

14. Bubble Flow Meter

Scheme 4.1 Flow diagram of CO_2 hydrogenation system

CHAPTER V

RESULTS AND DISCUSSION

This chapter is divided into two sections: 5.1) Characteristics of activated carbon derived from deoil rice bran residues under chemical activation and 5.2) Comparison of catalytic activity between Co-catalyst on various activated carbons for CO₂ hydrogenation,

5.1 Characteristics of activated carbon derived from deoil rice bran residues under chemical activation

5.1.1 Characteristics of rice bran residues

The rice bran residues used as raw materials to produce activated carbon in this study were the deoil rice brans from Thai Edible Co. Ltd., Ayuthaya, Thailand. The characteristics of rice bran residues were determined using the proximate analysis (ASTM D3173-D3175) and elemental analyzer (Perkin Elmer PE2400 Series II) shown in Tables 5.1 and 5.2, respectively.

Table 5.1 Proximate analysis results of deoil rice bran.

	Deoil rice bran
Moisture (%)	5.60
Ash content (%)	8.37
Volatile matter (%)	71.75
Fixed carbon (%)	14.28

Table 5.2 Elemental composition of deoil rice bran.

Composition (wt%)	Deoil rice bran
Carbon	38.02
Hydrogen	6.37
Nitrogen	3.31

5.1.2 Analysis of BET surface area and pore structure

From Figure 5.1, the tendency of BET surface area of activated carbons prepared from H_3PO_4 and ZnCl_2 activation at different activation temperatures was observed. For H_3PO_4 activation, the BET surface area slightly increases when the activation temperature increases from 400 to 500°C and reaches the maximum values at 500°C because the pores may not be fully developed at the lower temperature of 500°C. However, the BET surface area slightly decreases when the activation temperature increases from 500 to 700°C because of violent gasification reaction that may cause a part of the micropore structure to be destroyed by collapsing or combining together (Oh and Park, 2002). These results exhibit the similar trend as other researchers, who reported that the BET surface area of activated carbon from H_3PO_4 activation of rice husk (Liou and Wu, 2009) and wood (Hared et al., 2007) have the maximum at an activation temperature of 500 and 400°C, respectively. For ZnCl_2 activation, the BET surface area slightly decreases when the activation temperature increases from 400 to 700°C and has the maximum BET surface area at 400°C. In addition, the activated carbons from ZnCl_2 activation have higher BET surface areas than those of H_3PO_4 activation at the same activation temperature. These result is in agreement with other researchers (Timur, 2006; Liou, 2009). The maximum BET surface area of activated carbons are ca. 1400 m^2/g for ZnCl_2 activation and 1190 m^2/g for H_3PO_4 activation.

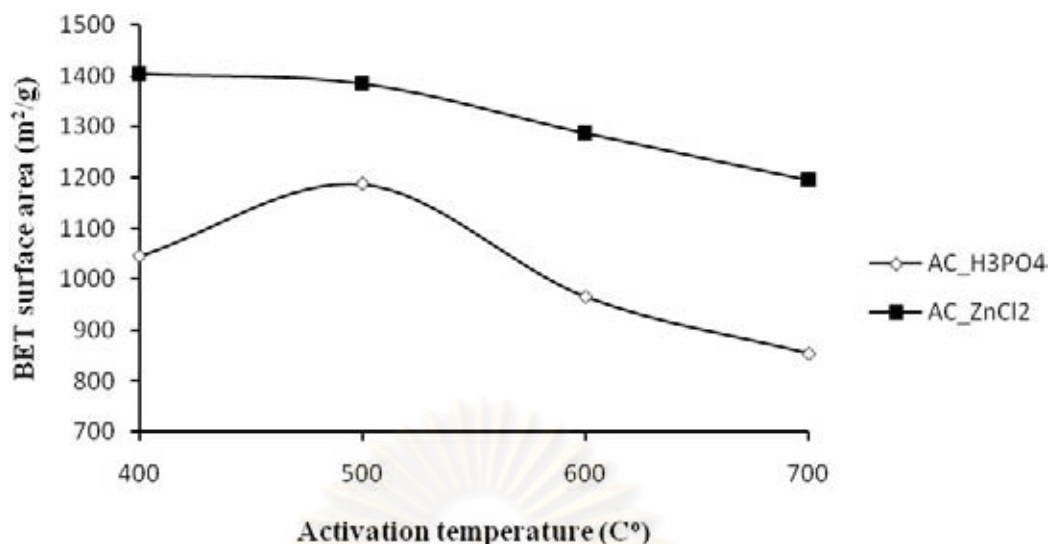


Figure 5.1 Effect of activation temperature on the surface area of activated carbons: ■, ZnCl₂ activation and ◇, H₃PO₄ activation

One of the methods for estimating the type of pores present in the activated carbons is to analyze the isotherm curve. The N₂ adsorption-desorption isotherms of the activated carbons prepared under different activation temperatures and kinds of activating agent are shown in Figure 5.2. The isotherms of the activated carbons prepared from deoil rice bran for both H₃PO₄ and ZnCl₂ activation exhibit a combination of types I and IV according to the IUPAC (International Union of Pure and Applied Chemistry) classification (Gregg and Sing, 1982). A combination of types I and IV isotherms are usually reflected the presence of both microporous and mesoporous structure. Figure 5.2(a) shows the isotherms of the activated carbons of H₃PO₄ activation at different activation temperatures. The isotherms exhibit a sudden increase in N₂ adsorption in the initial relative pressure range indicating the formation of micropores. In addition, the isotherms also appear to contain hysteresis loop at high relative pressure suggesting that the pore structure includes partly mesopores. So, the activated carbons of H₃PO₄ activation at different activation temperatures have both microporous and mesoporous structures (Liou, 2004). The adsorption capacity is at a maximum when the activation temperature is 500°C, indicating that the pore volume has the maximum amount at this temperature. Figure 5.2(b) shows the isotherms of the activated carbons of ZnCl₂ activation at different activation temperatures. These isotherms also exhibit the similar trend as seen with those from H₃PO₄ activation. These

adsorption isotherm behaviors indicate that samples have both micropores and mesopores structures. The highest adsorption capacity of the activated carbons of ZnCl_2 activation occurs at activation temperature of 400°C . In addition, the activated carbons of ZnCl_2 activation have the higher adsorption capacity than those of H_3PO_4 activation at the same activation temperature. These results are in accordance with those obtained from surface area.



ศูนย์วิทยทรัพยากร
จุฬาลงกรณ์มหาวิทยาลัย

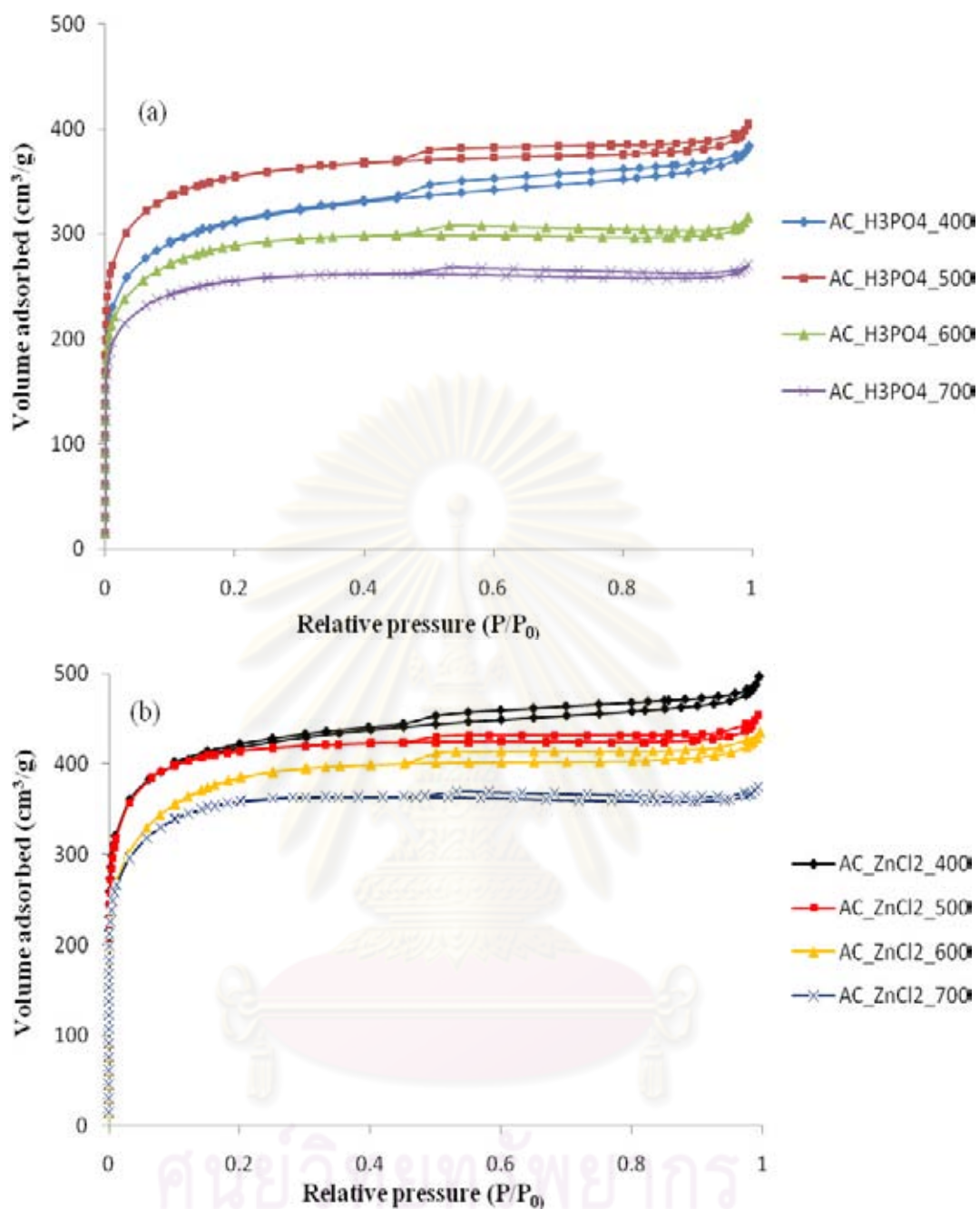


Figure 5.2 Adsorption-desorption isotherm of activated carbons at different activation temperature : (a) H₃PO₄ activation and (b) ZnCl₂ activation.

The characteristics of porosity of the activated carbon, such as the BET surface area, pore volume, average pore diameter are listed in Table 5.3. The pore volumes of ZnCl₂ activation have a value relatively higher than that of H₃PO₄ activation procedure. The maximum pore volume of activated carbons are 0.746 cm³/g for ZnCl₂ activation at the activation temperature of 400°C and 0.611 cm³/g for H₃PO₄ activation at the activation temperature of 500°C. In addition, the range of pore diameters of the activated

carbons that was calculated as $4V/A$ by BET method ranged from 1.905 to 2.126 nm for $ZnCl_2$ activation and 1.922 to 2.222 nm for H_3PO_4 activation. It was observed that the activated carbons with $ZnCl_2$ activation have a slightly smaller pore diameter than that of H_3PO_4 activation. These results are in agreement with other researchers (Liou and Wu, 2009).

Table 5.3 pore characteristics for activated carbons

	H_3PO_4 activation				$ZnCl_2$ activation			
	400	500	600	700	400	500	600	700
$S_{BET}(m^2/g)$	1045	1187	965	853	1404	1385	1288	1196
$V_t(cm^3/g)$	0.581	0.611	0.476	0.410	0.746	0.686	0.659	0.569
$V_{mic}(cm^3/g)$	0.463	0.55	0.464	0.409	0.633	0.653	0.609	0.568
$\%V_{mic}$	79.690	90.016	97.479	99.756	84.853	95.190	92.413	99.824
$D_p(nm)$	2.222	2.058	1.973	1.922	2.126	1.981	2.049	1.905

S_{BET} , BET surface area; V_t , total pore volume; V_{mic} , micropore volume; $\%V_{mic}$, $(V_{mic}/V_t)*100$; D_p , average pore diameter calculated as $4V/A$ by BET.

Pore size distributions of activated carbons by Horvath-Kawazoe method are shown in Figure 5.3. It is observed that most of pores for all samples were in the micropore range (< 2 nm). In addition, it is also noticed that the portion of pores for the activated carbons with $ZnCl_2$ activation having the range from 0.4 to 1.4 nm are higher than that of H_3PO_4 activation. As the result, BET surface area and micropore volume of the activated carbons for $ZnCl_2$ activation are higher than that of H_3PO_4 activation.

ศูนย์วิทยทรัพยากร
จุฬาลงกรณ์มหาวิทยาลัย

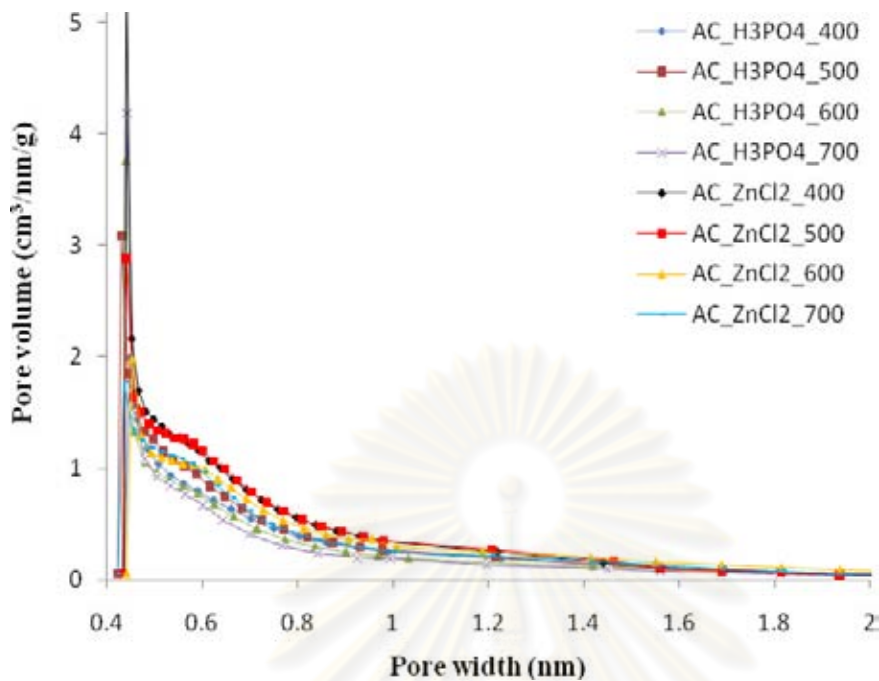


Figure 5.3 Pore size distribution of activated carbons by Horvath-Kawazoe method

5.1.3 Analysis of yield

The effect of activation temperature on the yield of activated carbons for both H_3PO_4 and ZnCl_2 activated samples is shown in Figure 5.4. The yield of activated carbons is calculated by using Equation 5.1. The standard deviations of the yield are in the order of ca. $\pm 2\%$, and these values are used as the basis for error bars shown in the Figure 5.4.

$$\text{Activated carbon yield (\%)} = \frac{\text{mass of activated carbon}}{\text{mass of deoil rice bran}} \times 100 \quad \dots (5.1)$$

Figure 5.4 shows that the yield of activated carbon for both H_3PO_4 and ZnCl_2 activation decreases when activation temperature increases. By increasing the activation temperature, the gasification reaction occurred severely, and ultimately leads to a reduction of the yield. The yield of activated carbon for ZnCl_2 activation are the same as that of activated carbon prepared from rice bran by physical activation procedure, which are 24.1-27.2 wt% (Suzuki et al., 2007). For the same activation temperature, the

yield of activated carbon for H_3PO_4 activation is relatively higher than that of ZnCl_2 activation.

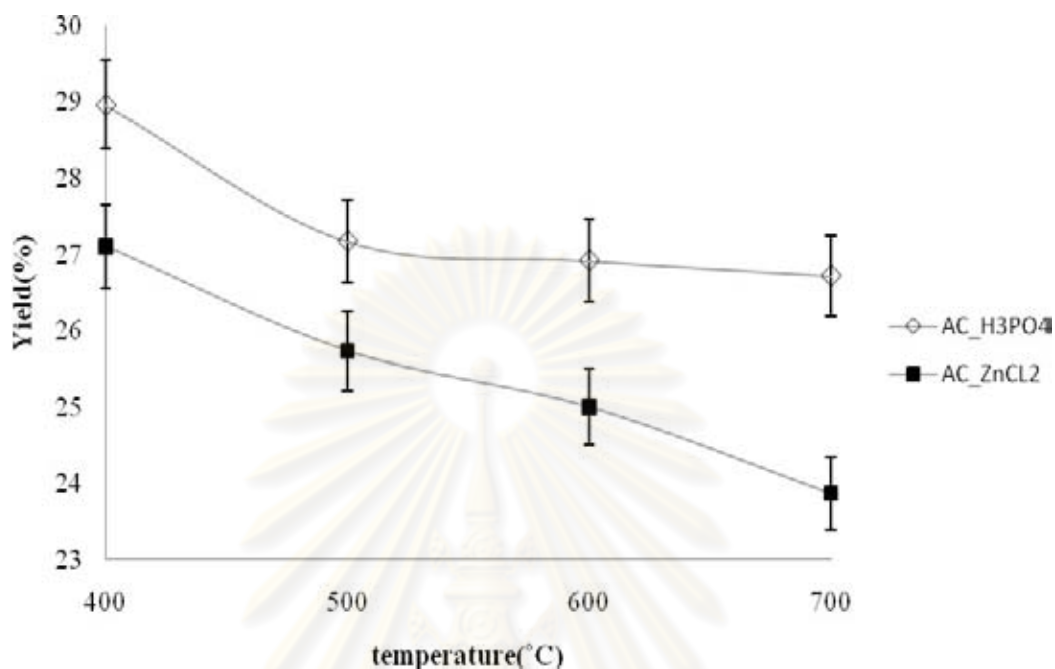


Figure 5.4 Effect of activation temperature on the yield of activated carbons: ■, ZnCl_2 activation and ◇, H_3PO_4 activation

5.1.4 Analysis of XRD

The XRD patterns of deoil rice bran and activated carbons obtained from ZnCl_2 and H_3PO_4 activation at different activation temperature are shown in Figure 5.5. The characteristic of the raw material has only a diffraction peak around $2\theta = 22.5^\circ$ as shown in Figure 5.5(a), being similar to the characteristic of silica in the rice husk (Liou et al., 1997). In addition, there are two broad peaks around $2\theta = 22.5^\circ$ and 45° for the activated carbons. Moreover, the broad peak around $2\theta = 45^\circ$ shows a narrowing when activation temperature increases, indicating an increase in the lattice size. The XRD patterns for both activated carbons obtained from H_3PO_4 and ZnCl_2 are similar upon identical calcination temperature.

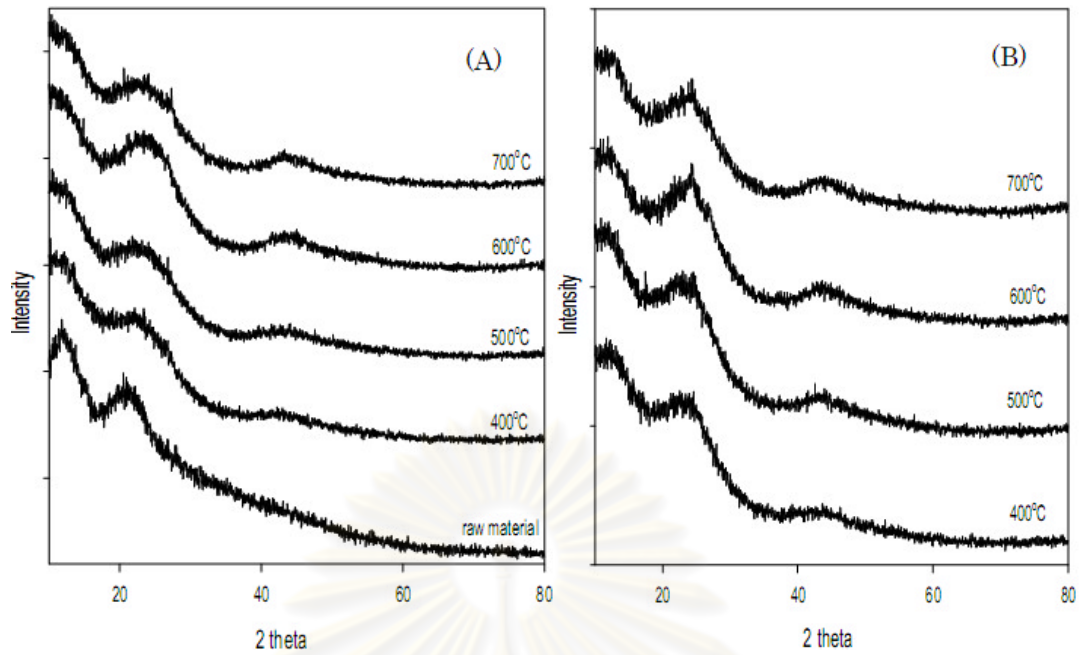


Figure 5.5. X-ray diffractogram of activated carbon at the different activation temperature and raw material: (A) ZnCl_2 activation and raw material and (B) H_3PO_4 activation.

5.1.5 Analysis of Scanning Electron Microscopy

The morphological features of the deoil rice bran, activated carbon from H_3PO_4 and ZnCl_2 activation are shown in Figure 5.6. For the deoil rice bran, the surface exhibits many thin sheets or layers within the structure. However, agglomeration and migration of inorganic matter that is present large amount on the surface of the raw material can be observed from SEM micrographs (Suzuki et al., 2007). This causes pore blockage. For activated carbons from both H_3PO_4 and ZnCl_2 activation, the activation process resulted in a substantial removal of inorganic material that can be seen in the micrographs.

จุฬาลงกรณ์มหาวิทยาลัย

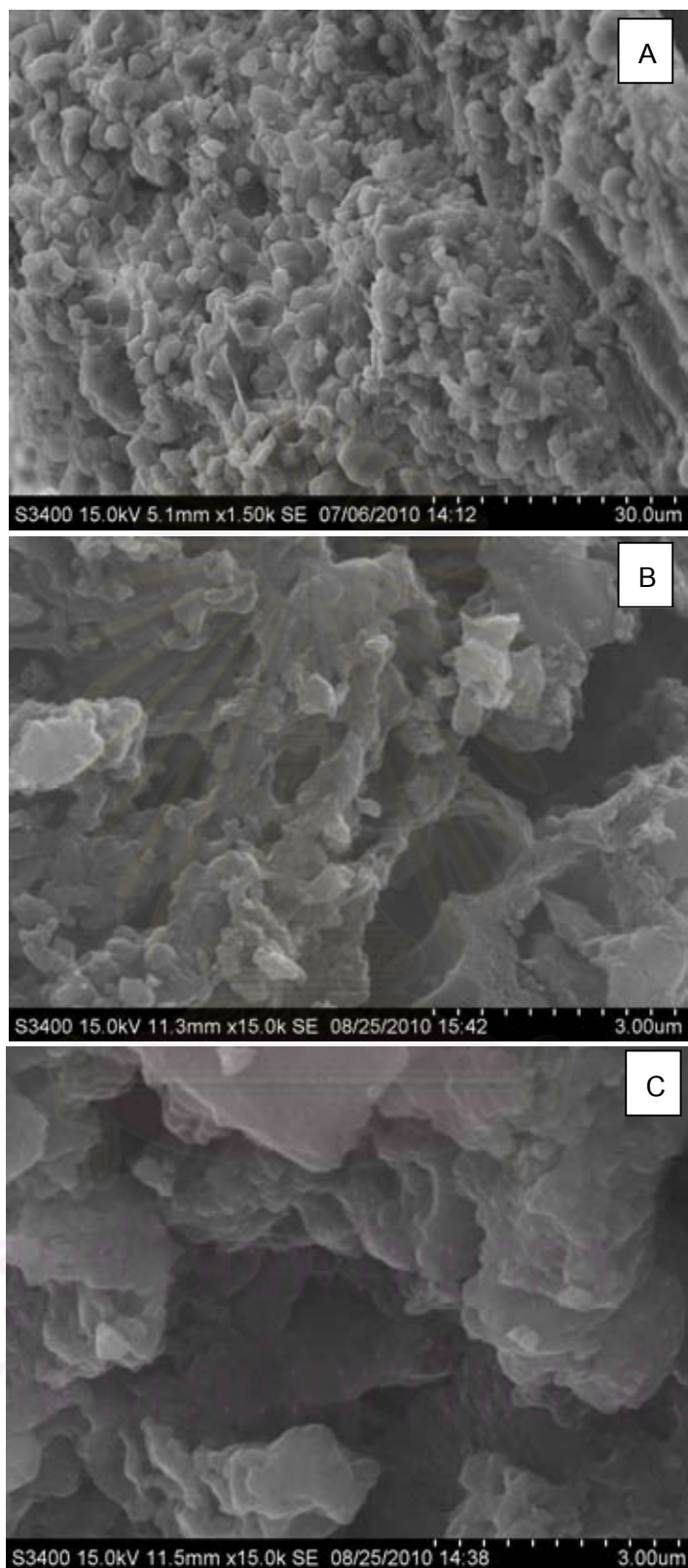
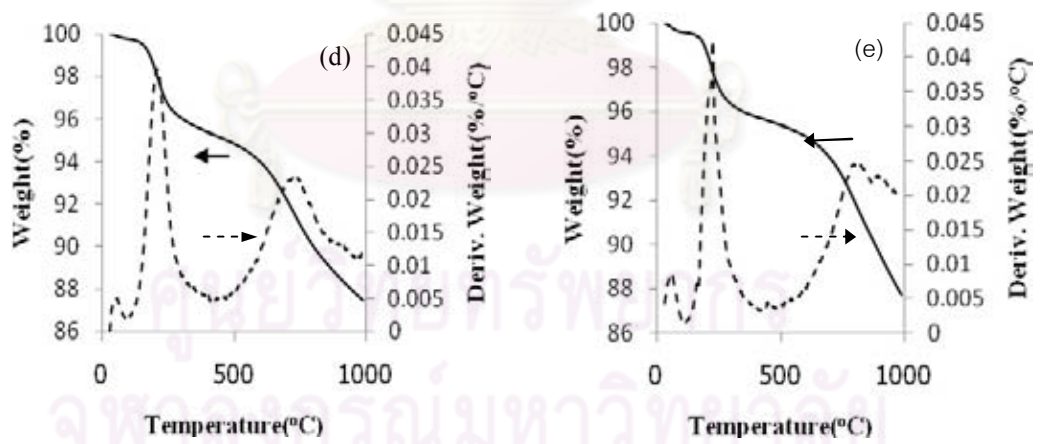
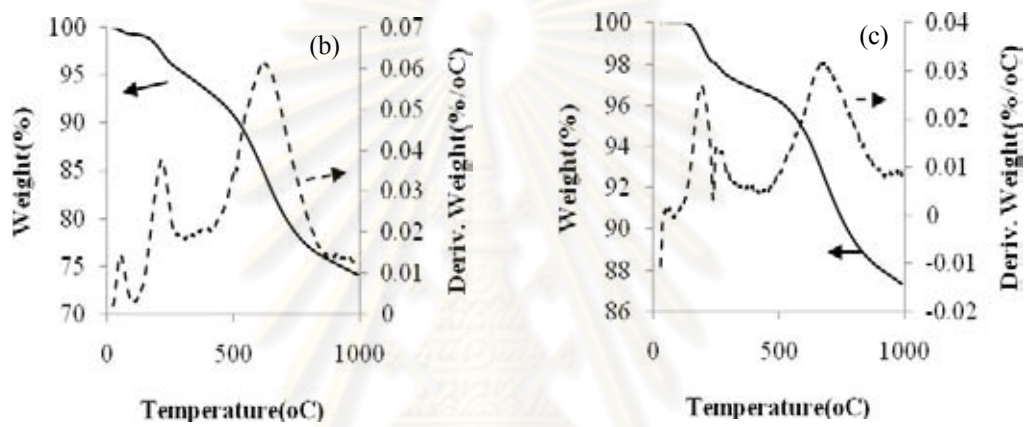
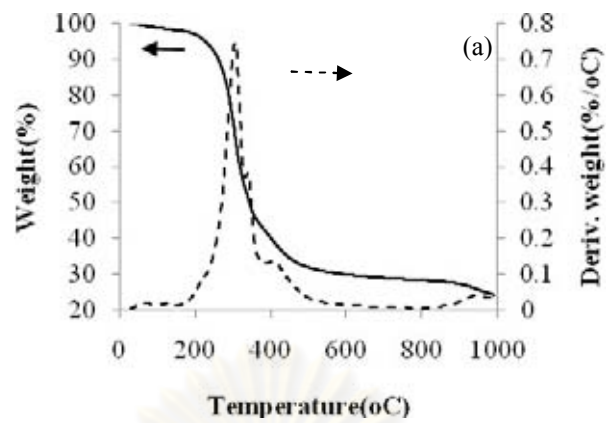


Figure 5.6: Scanning electron micrographs of samples: (A) raw material, (B) activated carbon by H_3PO_4 at 500°C , (C) activated carbon by ZnCl_2 at 500°C

5.1.6 Analysis of Thermal Gravimetric Analysis

The results of thermogravimetric analysis of deoil rice bran and activated carbons are presented in **Figure 5.7**. The mass loss during the thermogravimetric analysis can be divided into stages (Zerious, 1995; Orfao, 1999). **Figure 5.7(a)** shows the TGA and DTG curve of raw material. The first mass loss for temperature up to 200°C can be attributed to moisture elimination. The second stage (200<T<450 °C) can be attributed to the decomposition of organic materials that has a great mass loss (~60%). The third stage is found at 450–1000 °C range indicating decomposition of a structure with higher stability. These results have the similar trend as those of other researchers (Suzuki et al., 2007). **Figure 5.7(b)-5.7(e)** show the TGA and DTG curves of activated carbon for H₃PO₄ activation. The initial mass loss for temperature up to 200°C can be attributed to moisture elimination. The second stage is found at 200–300 °C range indicating the volatilization of organic materials. The third stage was found in the 300–600 °C range that may be attributed to further thermal decomposition of organic materials. Above 600°C, the mass loss may be attributed to the reaction between the activating agent and carbonaceous residue. These results are also in agreement with other researchers (Liou and Wu, 2009). **Figure 5.7(f)-5.7(i)** show the TGA and DTG curve of activated carbons for ZnCl₂ activation that have the similar trend as activated carbon with H₃PO₄ activation.



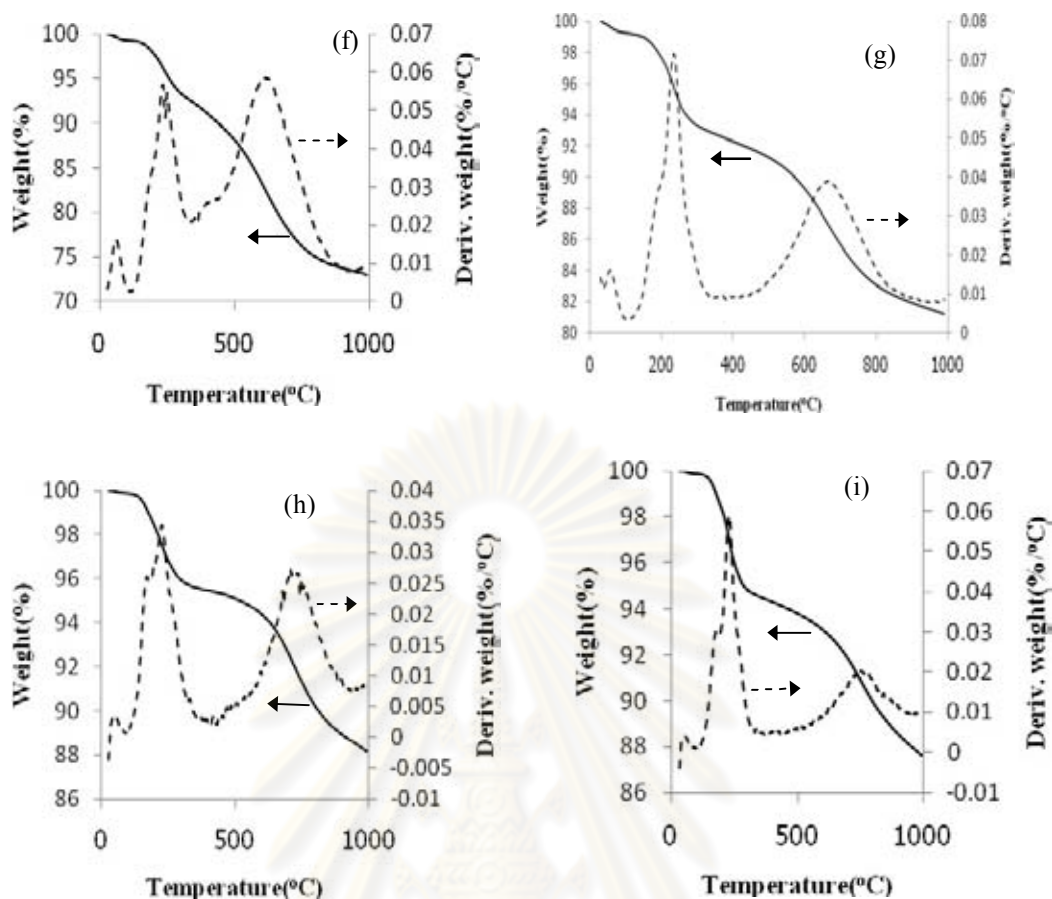


Figure 5.7 TG and DTG thermograms of samples: (a) deoil rice bran; H_3PO_4 activation samples at (b) 400°C , (c) 500°C , (d) 600°C , (e) 700°C ; and ZnCl_2 activation samples at (f) 400°C , (g) 500°C , (h) 600°C , (i) 700°C .

5.1.7 Analysis of impurity of activated carbons

The impurity of activated carbons that occurred from synthesis of activated carbons detected by X-ray fluorescence spectrometry (XRF) is shown in Table 5.4. It can be observed that high activation temperature resulted in high amounts of Phosphorus and Zinc remains.

Table 5.4 The impurity of activated carbons

Samples	Impurity (ppm)		
	P	Zn	S
AC_H ₃ PO ₄ _400	10,600	-	6,400
AC_H ₃ PO ₄ _500	23,100	-	7,500
AC_H ₃ PO ₄ _600	23,700	-	18,600
AC_H ₃ PO ₄ _700	30,400	-	11,600
AC_ZnCl ₂ _400	-	1,400	10,300
AC_ZnCl ₂ _500	-	1,600	33,900
AC_ZnCl ₂ _600	-	1,700	34,700
AC_ZnCl ₂ _700	-	1,700	46,200

5.2 Comparison of catalytic activity between Co-catalyst on various activated carbons for CO₂ hydrogenation

The study of this part focused on performance of the cobalt catalysts supported on various activated carbons for CO₂ hydrogenation. After synthesis, all catalyst samples were characterized by means of N₂ physisorption, XRD, SEM/EDX, CO chemisorptions, TEM, TPR, and TGA and were studied in reaction. The reaction study was carried out in CO₂ hydrogenation to determine the overall activity of the catalyst samples. First, the catalysts were reduced in H₂ at 400°C for 3 h in a fixed-bed flow reactor. Then, the reaction test was carried out with flow rate of H₂/CO₂/Ar = 20/2/8 cm³/min.

5.2.1 Analysis of BET surface area and pore structure

The characteristics of porosity of cobalt catalysts supported on various activated carbons, such as the BET surface area, pore volume, average pore diameter are listed in **Table 5.5**. From the result, it can be found that the surface areas and pore volume of activated carbons supported cobalt catalysts were less than those of activated carbons used as support, indicating that the pore blockage by cobalt clusters occurred.

Table 5.5 BET surface area, pore volume and average pore sizes of the Co-catalysts

Sample	BET surface area (m ² /g)	Pore volume (cm ³ /g)	Average pore size (nm)
Co/AC_H ₃ PO ₄ _400	35.9	0.021	2.36
Co/AC_H ₃ PO ₄ _500	376.4	0.162	1.73
Co/AC_H ₃ PO ₄ _600	511.3	0.261	2.04
Co/AC_H ₃ PO ₄ _700	590.8	0.273	1.85
Co/AC_ZnCl ₂ _400	36.4	0.016	1.71
Co/AC_ZnCl ₂ _500	355.91	0.191	2.14
Co/AC_ZnCl ₂ _600	617.6	0.291	1.88
Co/AC_ZnCl ₂ _700	748.6	0.345	1.84

5.2.2 Analysis of CO Chemisorption

The results of CO chemisorption for the catalyst samples are illustrated in **Table 5.6**. From the result, amount of active site of catalysts ranged from 1.51 to 2.73 ($\times 10^{19}$ site/g.cat), whereas, Co dispersion of catalysts ranged from 1.01 to 1.70%. Thus, Co exhibited well dispersion on supports.

Table 5.6 Active site, total CO-chemisorptions and %Co dispersion of the Co-catalysts.

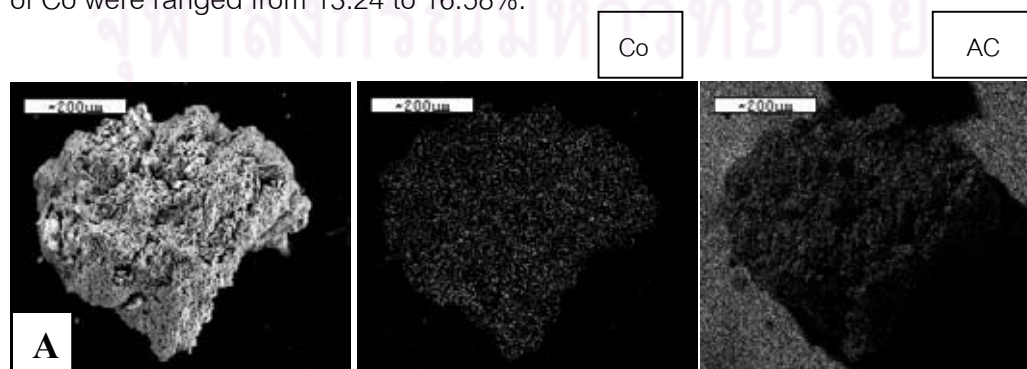
Sample	Co content ^a (%wt)	CO-pulse chemisorptions		
		Active site($\times 10^{-19}$ site/g.cat)	Total CO chemisorptions ($\mu\text{mol CO/g.cat}$)	%Co dispersion ^b
Co/AC_H ₃ PO ₄ _400	17.4	2.73	45.33	1.70
Co/AC_H ₃ PO ₄ _500	16.1	1.85	30.73	1.25
Co/AC_H ₃ PO ₄ _600	13.2	1.51	25.16	1.25
Co/AC_H ₃ PO ₄ _700	13.7	1.78	29.63	1.41
Co/AC_ZnCl ₂ _400	16.9	1.57	26.08	1.01
Co/AC_ZnCl ₂ _500	16.9	1.81	30.12	1.17
Co/AC_ZnCl ₂ _600	16.3	1.87	31.10	1.38
Co/AC_ZnCl ₂ _700	17.1	1.88	31.33	1.49

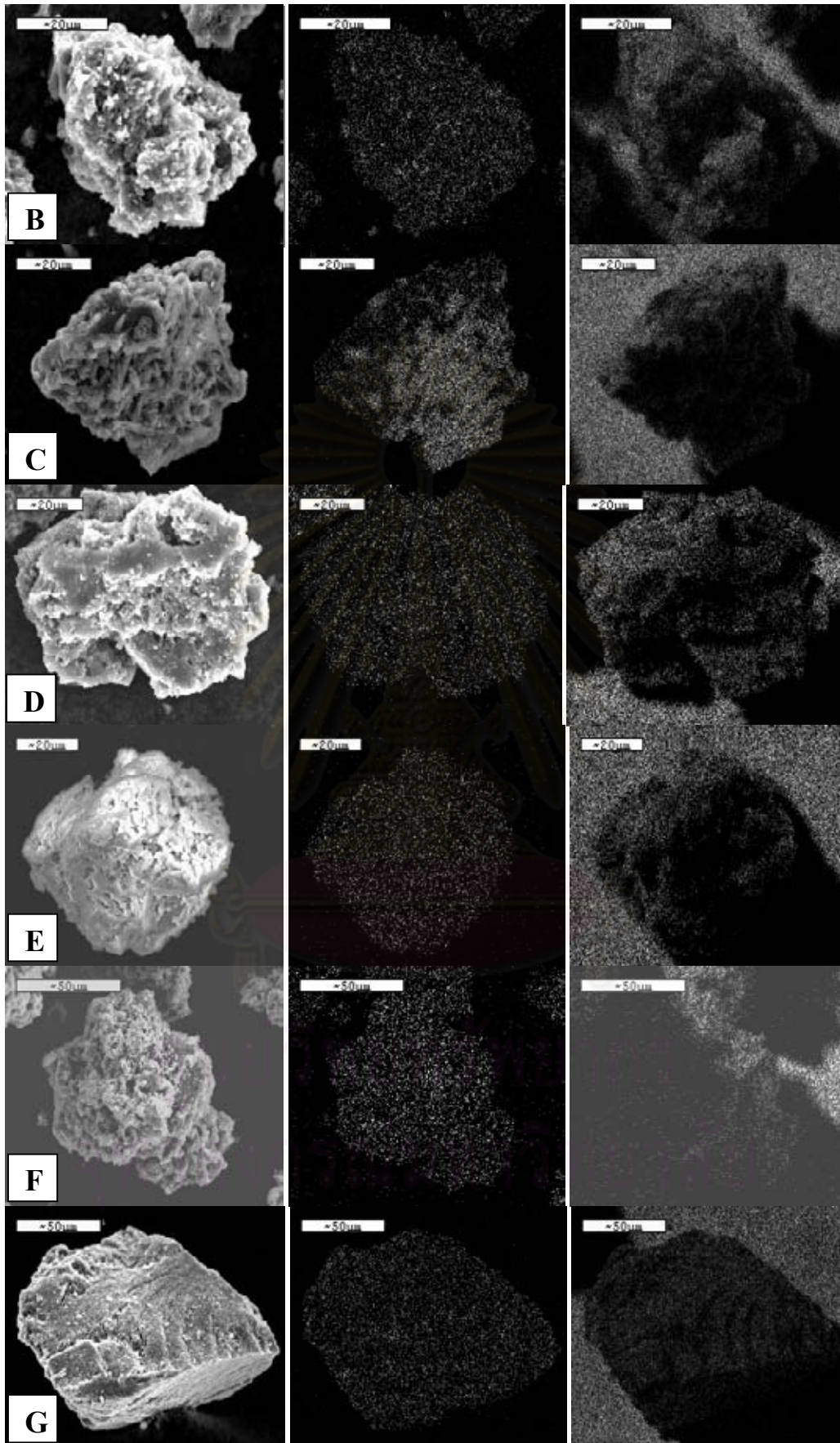
^a determined by ICP

^b based on Co content

5.2.3 Analysis of Scanning Electron Microscopy (SEM) and Energy Dispersive X-ray Spectroscopy (EDX)

Scanning electron microscopy (SEM) and energy dispersive X-ray spectroscopy (EDX) were also conducted in order to study the morphologies and elemental distribution of the samples, respectively. From **Figure 5.8**, it was found that all of Co-catalysts exhibited well dispersion of Co on the activated carbon. Energy dispersive X-ray spectroscopy (EDX) was performed in order to study elemental distribution (as shown in **Table 5.7**) of the sample in the bulk of catalysts. It was found that % elements of Co were ranged from 13.24 to 16.58%.





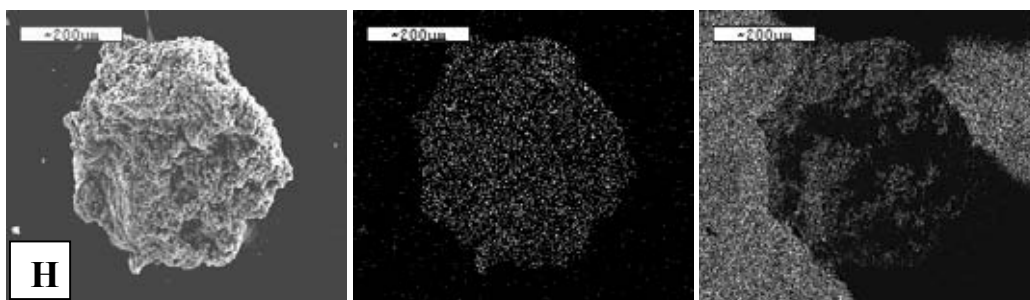


Figure 5.8 SEM/EDX images of Co-catalysts: (A)Co/AC_H₃PO₄_400, (B)Co/AC_H₃PO₄_500, (C)Co/AC_H₃PO₄_600, (D)Co/AC_H₃PO₄_700, (E) Co/AC_ZnCl₂_400, (F)Co/AC_ZnCl₂_500, (G)Co/AC_ZnCl₂_600, (H)Co/AC_ZnCl₂_700.

Table 5.7 EDX analysis of cobalt catalysts.

Samples	% Element			% Atomic		
	Co	C	O	Co	C	O
Co/AC_H ₃ PO ₄ _400	14.16	56.09	29.75	3.55	68.98	27.47
Co/AC_H ₃ PO ₄ _500	13.40	59.90	26.70	3.30	72.46	24.24
Co/AC_H ₃ PO ₄ _600	13.32	53.24	33.44	3.28	72.27	24.55
Co/AC_H ₃ PO ₄ _700	13.42	62.75	23.84	3.28	75.26	21.46
Co/AC_ZnCl ₂ _400	13.87	56.13	30.00	3.47	68.89	27.65
Co/AC_ZnCl ₂ _500	13.24	49.69	37.07	3.37	71.73	24.90
Co/AC_ZnCl ₂ _600	13.78	49.67	36.55	3.51	62.15	34.34
Co/AC_ZnCl ₂ _700	16.58	58.42	25.00	4.19	72.51	23.29

5.2.4 Analysis of Transmission Electron Microscopy (TEM)

TEM micrographs of activated carbons-supported Co catalysts are shown in Figures 5.9. For cobalt catalysts, the dark patches represented cobalt species dispersing on Co/AC_H₃PO₄_400 (a), Co/AC_ZnCl₂_400 (b) and Co/AC_ZnCl₂_700 (c).

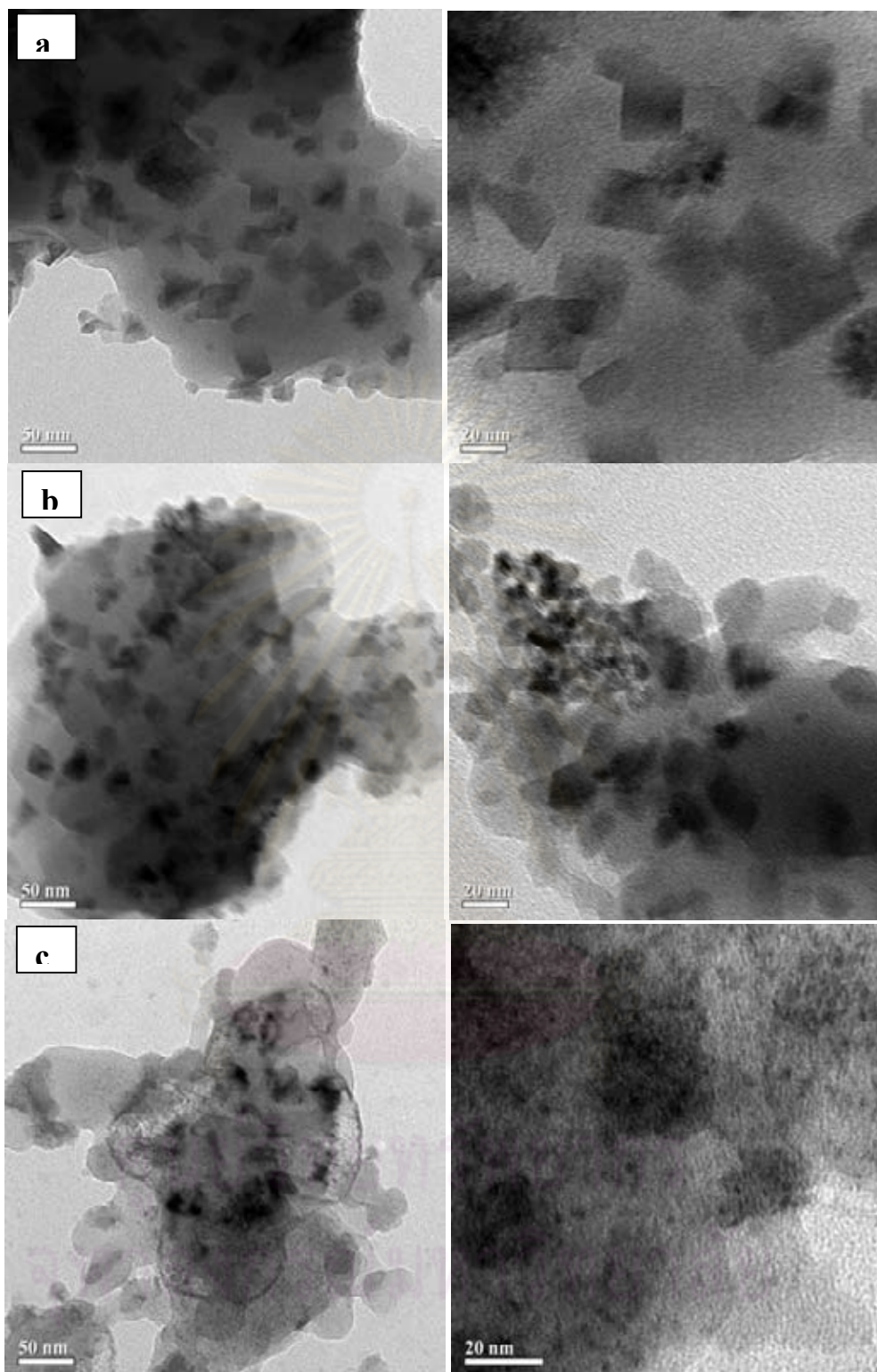


Figure 5.9 TEM images of AC-supported Co catalysts: (a)Co/AC_H₃PO₄_400, (b)Co/AC_ZnCl₂_400, (c)Co/AC_ZnCl₂_700

5.2.5 Analysis of X-ray diffraction (XRD)

XRD patterns of the Co-catalysts are shown in Figure 5.10. For some catalysts, the XRD peaks of Co_3O_4 and CoO were slightly observed at 36.8 and 42.5; respectively. This was probably due to Co oxide species were present in highly dispersed form.

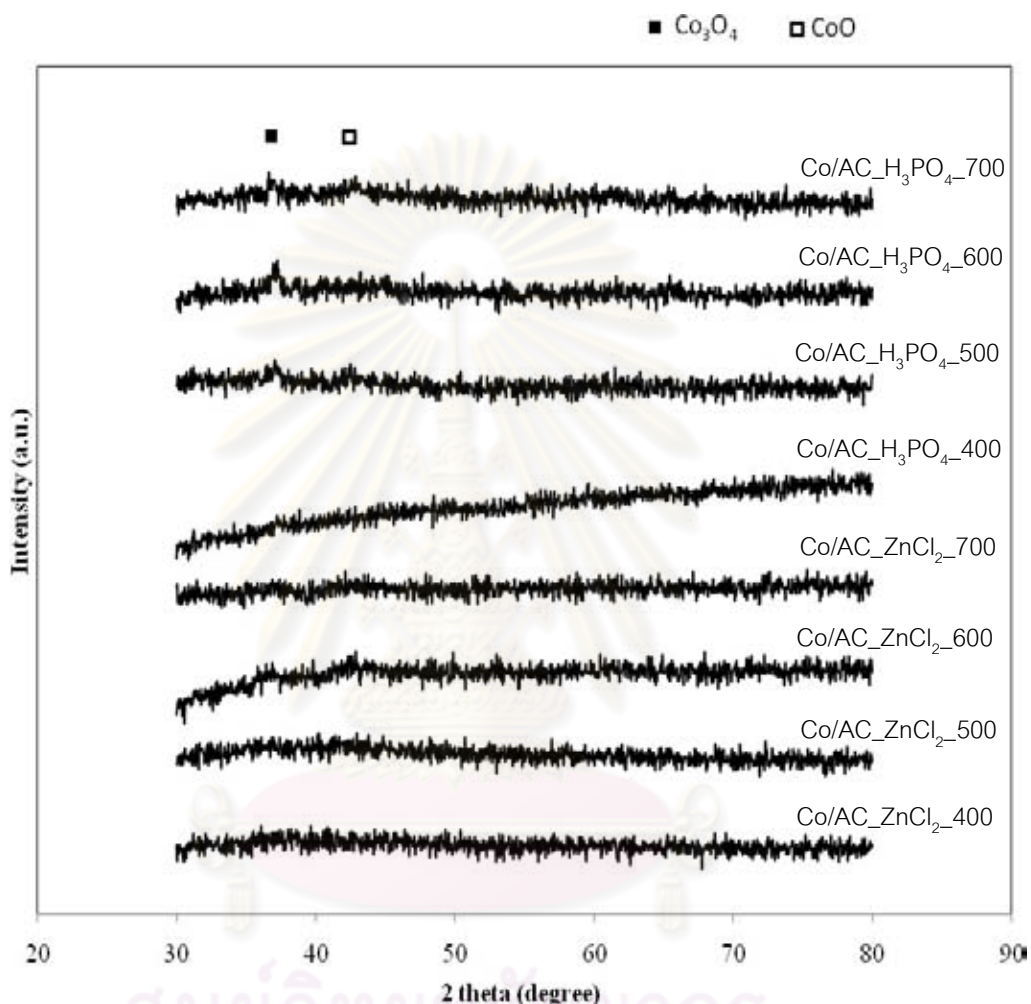
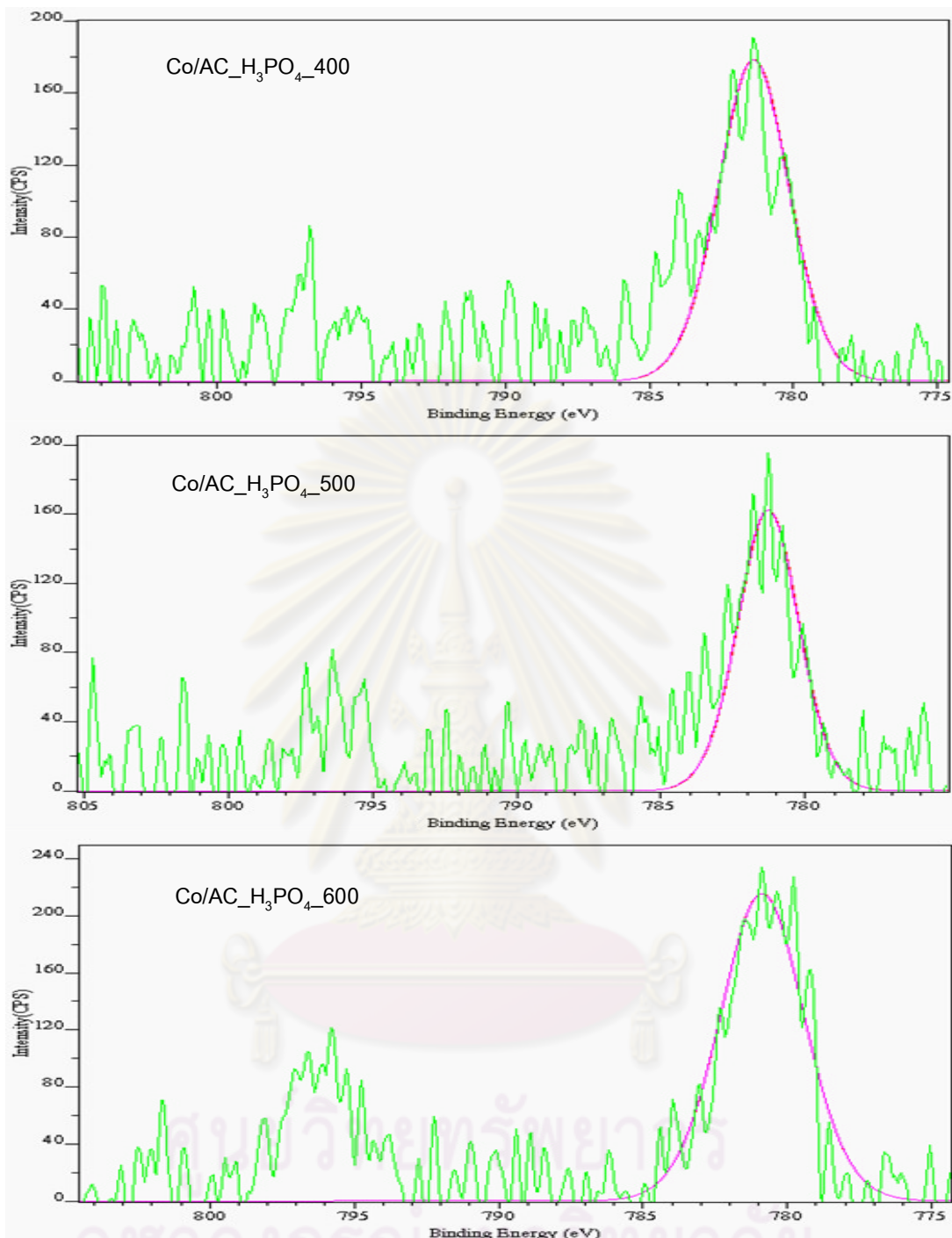


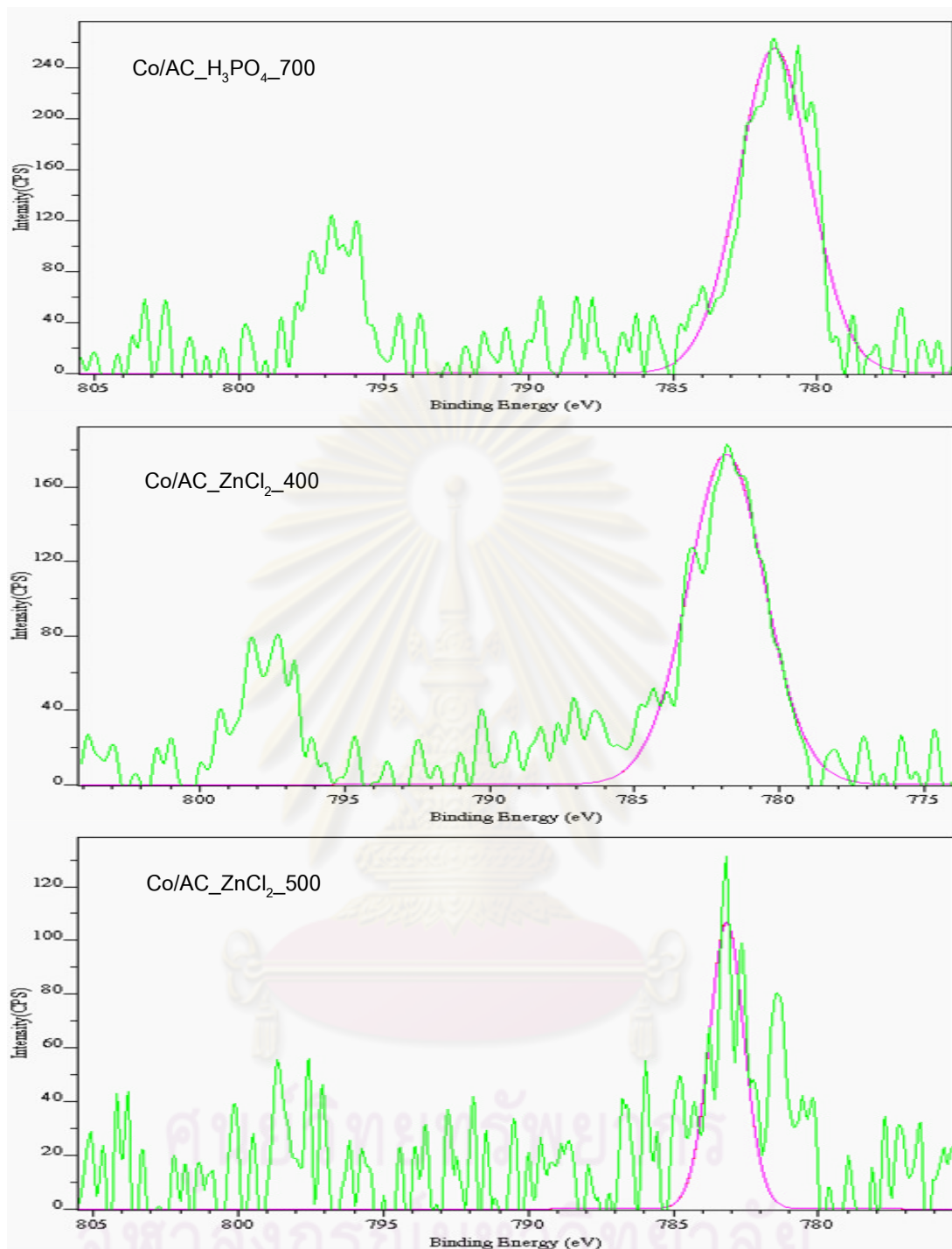
Figure 5.10 XRD patterns of Co catalysts

5.2.6 X-ray photoelectron spectroscopy

XPS analysis was carried out to determine the state of Cobalt. The samples were analyzed in the Co 2p with regards to the binding energy regions. The binding energy and FWHM of Co $2p_{3/2}$ is given in Table 5.8. The binding energies of Co $2p_{3/2}$ for all catalysts were consistent with that of Co^{2+} (J.Pola et al, 2010). The deconvoluted XPS spectra for the Co $2p_{3/2}$ core level region of cobalt catalysts are shown in Figures 5.11.



ศูนย์วิจัยทรัพยากร
จุฬาลงกรณ์มหาวิทยาลัย



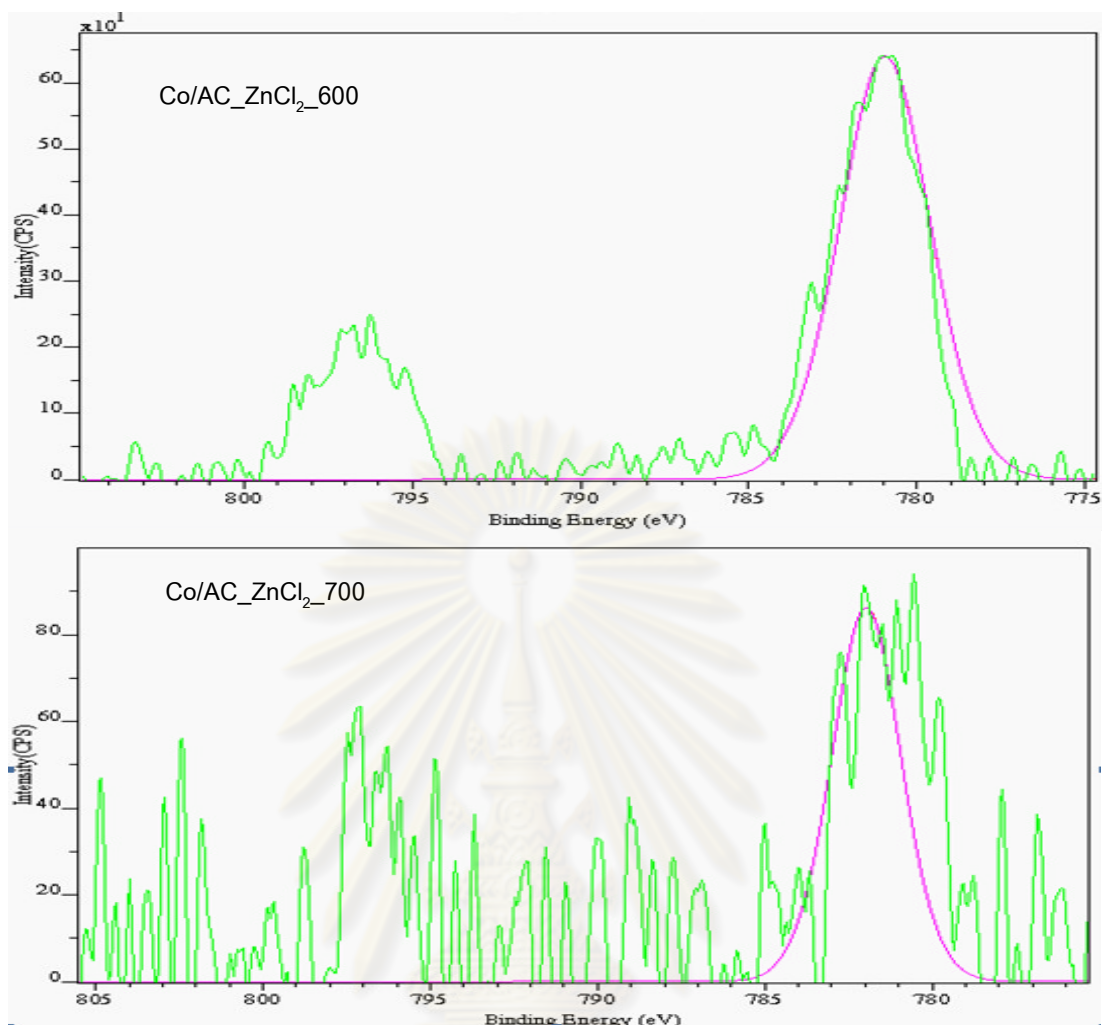


Figure 5.11 The deconvolution of Co2p_{3/2} of XPS spectra of Co-catalysts.

ศูนย์วิทยทรัพยากร
จุฬาลงกรณ์มหาวิทยาลัย

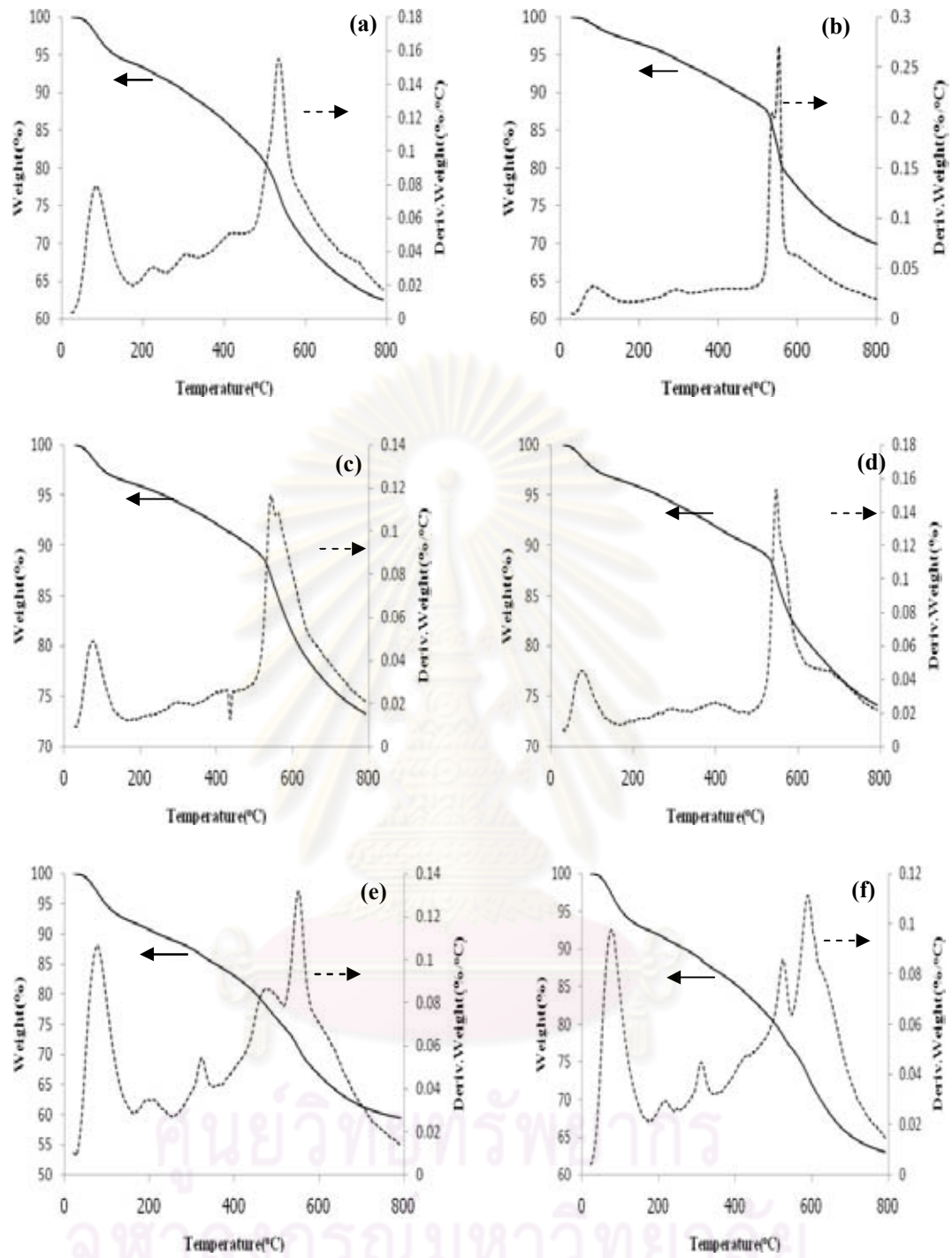
Table 5.8 The binding energy and FWHM of Co

Samples	Co(II) 2p _{3/2}	
	B.E. (eV)	FWHM
Co/AC_H ₃ PO ₄ _400	781.4	2.850
Co/AC_H ₃ PO ₄ _500	781.3	2.447
Co/AC_H ₃ PO ₄ _600	780.9	3.367
Co/AC_H ₃ PO ₄ _700	781.5	2.891
Co/AC_ZnCl ₂ _400	781.8	3.080
Co/AC_ZnCl ₂ _500	783.2	1.375
Co/AC_ZnCl ₂ _600	780.9	3.135
Co/AC_ZnCl ₂ _700	782.0	1.822
^a Co	778.1 ± 0.1	
^a CoO	780.1 ± 0.9	
^a Co ₃ O ₄	780.0 ± 0.7	
^b Co ²⁺	781.2	

^aL.Ji et al, 2000^bJ.Pola et al, 2010

5.2.7 Analysis of Thermal Gravimetric Analysis

The results of thermogravimetric analysis of activated carbons-supported cobalt catalysts are presented in **Figure 5.12**. The mass loss during the thermogravimetric analysis can be divided into stages. **Figure 5.12(a)-5.12(e)** show the TGA and DTG curves of cobalt catalysts supported on activated carbons treated using H₃PO₄ activation. The initial mass loss for temperature up to 200°C can be attributed to moisture elimination. The second stage is found at 200–500 °C range indicating the decomposition of cobalt nitrate. Above 500°C, the mass loss may be attributed to the reaction between the cobalt and carbonaceous residue. **Figure 5.12(e)-5.12(h)** show the TGA and DTG curves of cobalt catalysts supported on activated carbons treated using ZnCl₂ activation that have the similar trend as cobalt catalysts supported on activated carbons treated using H₃PO₄ activation.



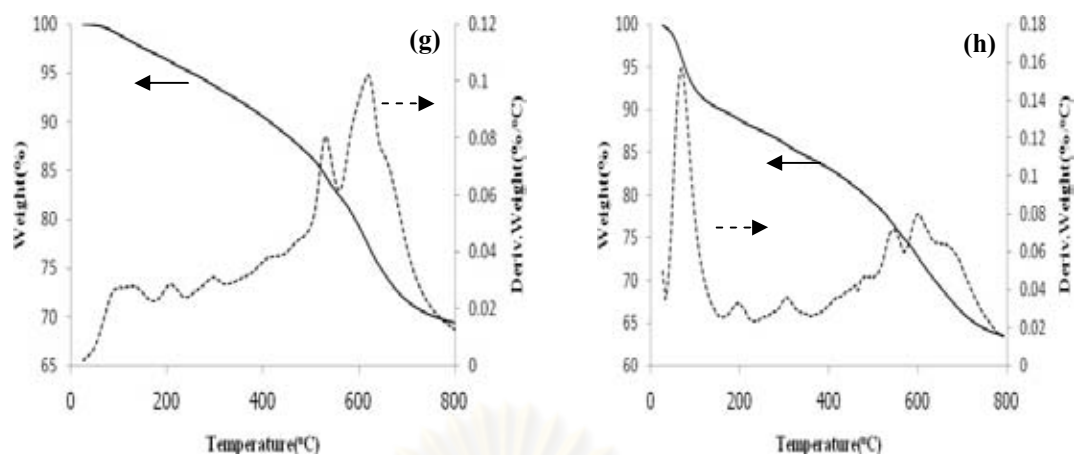


Figure 5.12 TG and DTG thermograms of Co catalysts: (a)Co/AC_H₃PO₄_400, (b)Co/AC_H₃PO₄_500, (c)Co/AC_H₃PO₄_600, (d)Co/AC_H₃PO₄_700, (e) Co/AC_ZnCl₂_400, (f)Co/AC_ZnCl₂_500, (g)Co/AC_ZnCl₂_600, (h)Co/AC_ZnCl₂_700.

5.2.8 Analysis of Temperature-programmed reduction (TPR)

The TPR profiles of all Co-catalysts are given in Figure 5.13. For cobalt catalysts supported on activated carbons treated using H₃PO₄ activation, the reduction temperature around 350°C was observed, which can be assigned to the reduction of Co₃O₄ to CoO. In addition, the reduction temperature around 450°C was also observed, which can be assigned to the reduction of CoO to Co. For cobalt catalysts supported on activated carbons treated using ZnCl₂ activation, the reduction temperature around 396°C was observed for Co/AC_ZnCl₂_400, which can be assigned to the reduction of Co₃O₄ to CoO. In addition, the reduction temperature around 442°C was also observed, which can be assigned to the reduction of CoO to Co. However, Co/AC_ZnCl₂_500, Co/AC_ZnCl₂_600 and Co/AC_ZnCl₂_700 only exhibited the reduction temperature around 410 °C, which may be caused by the presence of higher amounts of Zn residues that was present as seen in Table 5.4.

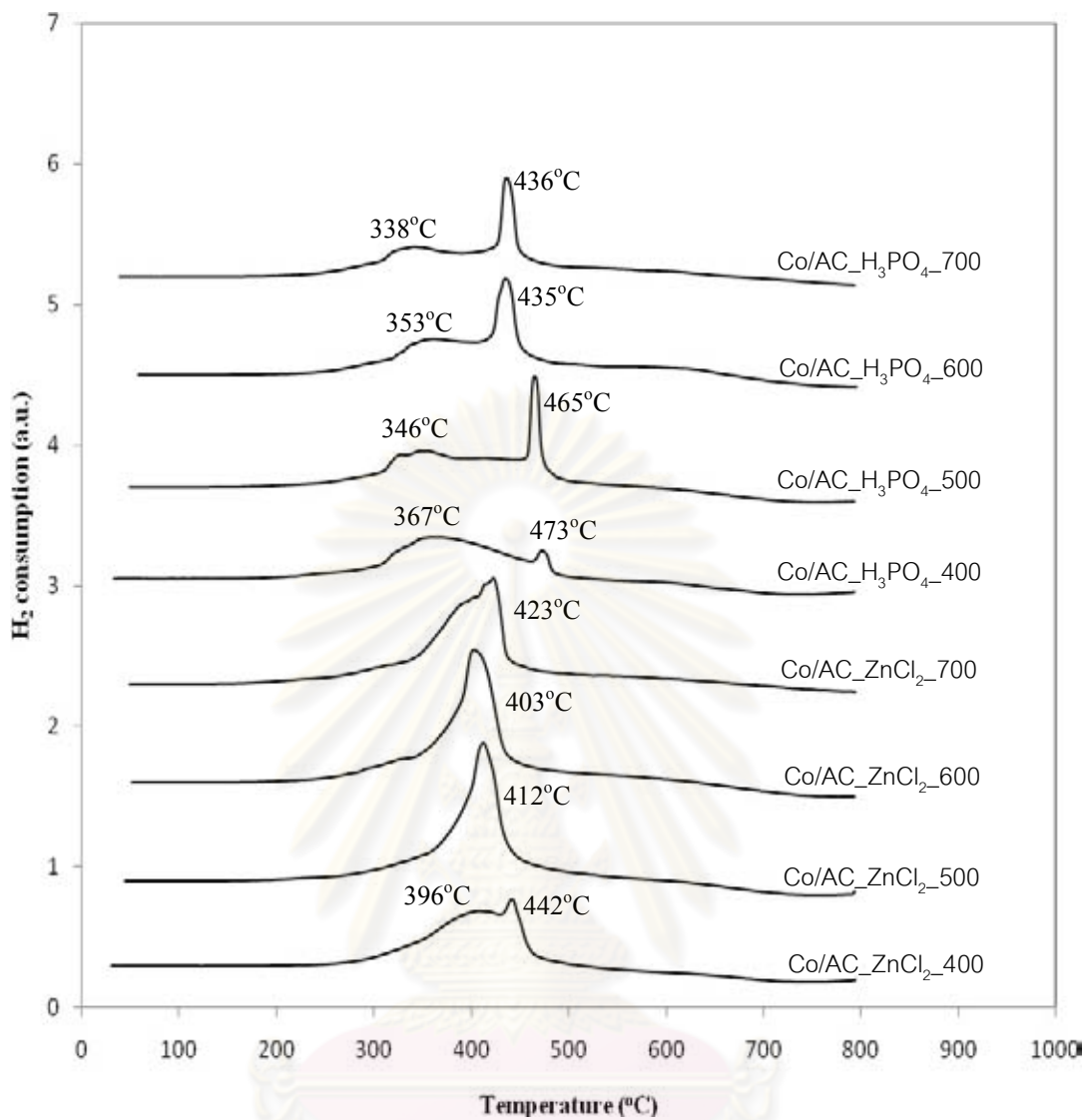


Figure 5.13 Reduction behaviors of the Co-catalysts.

ศูนย์วิทยทรัพยากร
จุฬาลงกรณ์มหาวิทยาลัย

5.2.9 Study of CO₂ hydrogenation

The conversion, reaction rate, product selectivity, TOF (based on the number of active sites measured from CO chemisorption) are shown in **Table 5.9** and the rate vs. time on stream of the cobalt catalysts are given in **Figure 5.14** in order to determine the catalytic behaviors of the Co supported on various activated carbons for CO₂ hydrogenation. It was found that the rate of reaction and the steady state conversion of activated carbon supported cobalt catalysts were in the order: Co/AC_H₃PO₄-400 > Co/AC_ZnCl₂-400 > Co/AC_H₃PO₄-500 > Co/AC_H₃PO₄-700 > Co/AC_H₃PO₄-600. In addition, this reaction did not occur for Co/AC_ZnCl₂-500, Co/AC_ZnCl₂-600 and Co/AC_ZnCl₂-700. These phenomena may be caused by sulfur impurity in supports that was shown in **Table 5.4**. Amounts of sulfur impurity of AC_ZnCl₂-500, AC_ZnCl₂-600 and AC_ZnCl₂-700 are 3.39%, 3.47% and 4.62%, respectively that were much enough to decrease the reaction. Whereas, amount of sulfur impurity of AC_H₃PO₄-400, AC_ZnCl₂-400, AC_H₃PO₄-500, AC_H₃PO₄-700 and AC_H₃PO₄-600 are 0.64%, 1.03%, 0.75%, 1.16% and 1.86%, respectively, this indicated that the conversion decreased with increased sulfur impurity. The conversion of Co/AC_H₃PO₄-500 was less than that of Co/AC_ZnCl₂-400, although the amount of sulfur impurity of AC_H₃PO₄-500 was higher than that of AC_ZnCl₂-400. This may be due to effect of P residues in AC_H₃PO₄-500.

Table 5.9 The conversion, reaction rate, product selectivity and TOF during CO₂ hydrogenation for Co catalysts

Catalysts	Rate ^c (x10 ² gCH ₂ /g cat.h)	Conversion ^a		Product selectivity ^c (%)		TOF ^d (x10 ³ s ⁻¹)
		Initial ^b	Steady state ^c	CH ₄	CO	
Co/AC_H ₃ PO ₄ _400	20.33	31.78	29.27	29.25	70.75	5.2
Co/AC_H ₃ PO ₄ _500	15.95	23.09	23.78	16.24	83.76	4.6
Co/AC_H ₃ PO ₄ _600	2.92	2.31	4.31	5.53	94.47	1.9
Co/AC_H ₃ PO ₄ _700	6.8	8.31	9.22	4.08	95.92	1.2
Co/AC_ZnCl ₂ _400	18.39	25.19	26.84	27.3	72.18	8.7
Co/AC_ZnCl ₂ _500	n.d.	n.d.	n.d.	n.d.	n.d.	n.d.
Co/AC_ZnCl ₂ _600	n.d.	n.d.	n.d.	n.d.	n.d.	n.d.
Co/AC_ZnCl ₂ _700	n.d.	n.d.	n.d.	n.d.	n.d.	n.d.

^a CO₂ hydrogenation was carried out at 270 °C, 1 atm, and H₂/CO₂/Ar = 10/1/4, GSHV= 11400 h⁻¹.

^b After 5 min of reaction.

^c After 5 h of reaction.

^d The TOF calculation was based on CO chemisorptions

n.d. = not detected

ศูนย์วิทยทรัพยากร
จุฬาลงกรณ์มหาวิทยาลัย

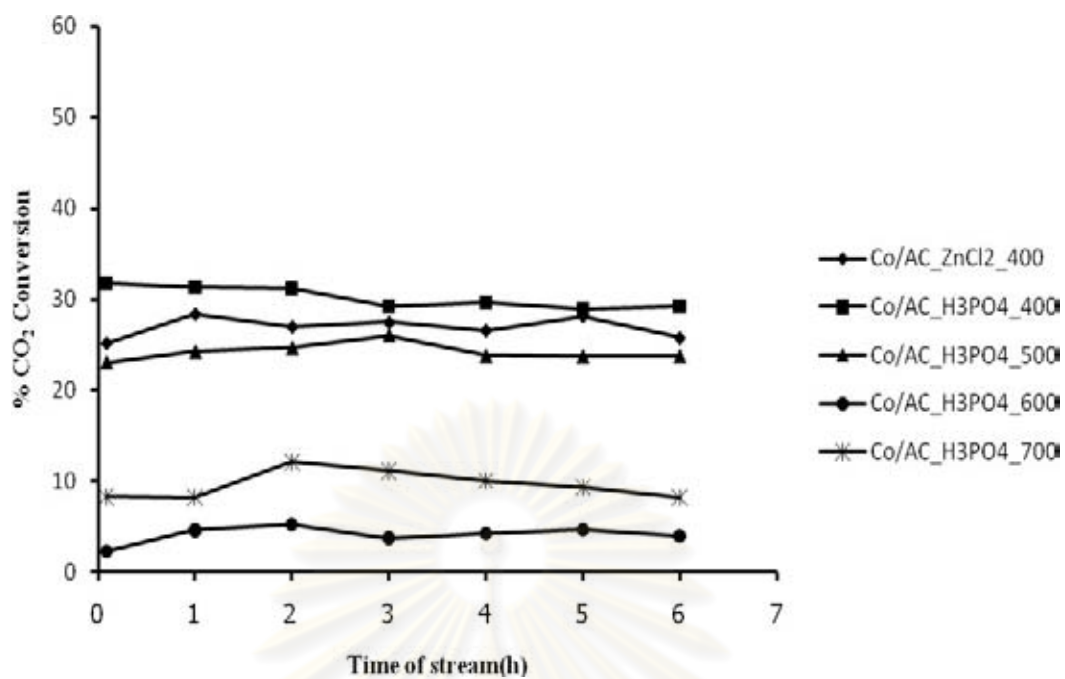


Figure5.14 The rate vs. time of stream of the cobalt catalysts

ศูนย์วิทยทรัพยากร
จุฬาลงกรณ์มหาวิทยาลัย

CHAPTER VI

CONCLUSIONS AND RECOMMENDATIONS

6.1 Conclusions

6.1.1 Characteristics of activated carbon derived from deoil rice bran residues under chemical activation

This study reports the preparation of activated carbon from rice bran residues using H_3PO_4 and ZnCl_2 as the chemical activating agents. Summary is given as follows:

- 1) The ZnCl_2 activation produces a higher surface area than the H_3PO_4 activation for preparation of activated carbon.
- 2) The maximum surface area of $1404 \text{ m}^2/\text{g}$ for ZnCl_2 activation at the activation temperature of 400°C and the maximum surface area of $1187 \text{ m}^2/\text{g}$ for H_3PO_4 activation at the activation temperature of 500°C are achieved.
- 3) The activated carbons for both H_3PO_4 and ZnCl_2 activation exhibit a combination of mostly microporous and partly mesoporous structure.
- 4) The high surface area of carbon obtained from rice bran residues is comparable to that of other lignin–cellulose matter. So, rice bran residues can be used as promising material in the activated carbon preparation process.

6.1.2 Comparison of catalytic activity between Co catalysts on various activated carbons for CO_2 hydrogenation

This study reports the comparison of performance of various activated carbons used as supports of Co catalysts for CO_2 hydrogenation. Summary is given as follows:

- 1) Amounts of sulfur impurity from using H_2SO_4 for treating in preparation of activated carbon from rice bran residues affects to catalytic performance.

- 2) The conversion and CH_4 selectivity obtained from using these activated carbons as supports of Co catalysts are poor for methanation, but being better for the reverse water gas shift reaction.
- 3) The conversion for Co/AC_ H_3PO_4 -400 catalyst reaches the highest among other catalysts because it contains the least amounts of sulfur impurity.

6.2 Recommendations

- 1) Trying to find the new method for the preparation of activated carbon from rice bran residues in order to obtain suitable property for leading to use.
- 2) Sulfur impurity obtained from using H_2SO_4 for treating in preparation of activated carbon should be investigated and eliminated in order to improve performance of catalyst.
- 3) These activated carbons having high surface area can be used for other reaction that may exhibit a good performance, such as Pd/AC for hydrodechlorination, etc.
- 4) These activated carbons may be suitable to be support for ZrO_2 in biodiesel process because these activated carbons have acidity that will improve performance of ZrO_2 .

REFERENCES

- Ahmadpour, A., and Do, D. D. The preparation of active carbons from coal by chemical and physical activation. Carbon. 34 (1996): 471-479.
- Arakawa, H., et al. Catalysis research of relevance to carbon management: Progress, Challenges, and Opportunities. Chemical Review 101 (2001): 953-996.
- Azevedo, D. C. S., et al. Microporous activated carbon prepared from coconut shell using chemical activation with zinc chloride. Microporous and Mesoporous Materials 100 (2007): 361–364.
- Bando, K. K., Sayama, K., Kusama, H., Okabe, K., and Arakawa, H. In-situ FT-IR study on CO₂ hydrogenation over Cu catalysts supported on SiO₂, Al₂O₃ and TiO₂. Applied Catalysis A 165 (1997): 391-409.
- Basta, A. H., Fierro, V., El-Saied, H., and Celzard, A. 2-Steps KOH activation of rice straw: An efficient method for preparing high-performance activated carbons. Bioresource Technology 100 (2009): 3941–3947.
- Bedia, J., Rosas, J. M., Mirasol, J. R., and Cordero, T. Pd supported on mesoporous activated carbons with high oxidation resistance as catalysts for toluene oxidation. Applied Catalysis B Environmental 94 (2010): 8–18.
- Castilla, C. M., and Marin, F. C. Cobalt catalysts supported on activated carbons: Preparation and Behavior in the hydrogenation of carbon oxides. Journal of the Chemical Society Faraday Transactions 91(19) (1995): 3519-3524.
- Chang, F. W., Hsiao, T. J., Chung, S. W., and Lo, J. J. Nickel supported on rice husk ash — activity and selectivity in CO₂ methanation. Applied Catalysis A: General 164 (1997): 225-236.
- Chitra, S., Sekaranb, G., and Chandrakasan, G. Adsorption of a mutant strain of *Pseudomonas pictorum* on rice bran based activated carbon. Journal of Hazardous Materials 48 (1996): 239-250.

- Chen, C. S., Cheng, W. H., and Lin, S. S. Study of reverse water gas shift reaction by TPD, TPR and CO₂ hydrogenation over potassium-promoted Cu/SiO₂ catalyst. Applied Catalysis A: General 238 (2003): 55-67.
- Daifullah, A. A. M., Girgis, B. S., and Gad, H. M. H. Utilization of agro-residues (rice husk) in small waste water treatment plans. Materials Letters 57 (2003): 1723– 1731.
- Dorner, R. W., Hardy, D. R., Williams, F. W., Davis, B. H., and Willauer, H. D. Influence of gas feed composition and pressure on the catalytic conversion of CO₂ to hydrocarbons using a traditional cobalt-based Fischer-Tropsch catalyst. Energy & Fuels 23 (2009): 4190-4195.
- Dutta, P., Elbashir, N. O., Manivannan, A., Seehra, M. S., and Roberts, C. B. Characterization of Fischer-Tropsch cobalt-based catalytic systems (Co/SiO₂ and Co/Al₂O₃) by X-ray diffraction and magnetic measurements. Catalysis letters 98 (2004): 203-210.
- Faria, P. C. C., Monteiro, D. C. M., Órfão, J. J. M., and Pereira, M. F. R. Cerium, manganese and cobalt oxides as catalysts for the ozonation of selected organic compounds Chemosphere 74 (2009): 818–824.
- Fisher, I. A., and Bell, A. T. *In-Situ* Infrared Study of Methanol Synthesis from H₂/CO₂ over Cu/SiO₂ and Cu/ZrO₂/SiO₂. Journal of Catalysis 172 (1997): 222-237.
- Gu, J. Y., Li, K. X., Wang, J., and He, H. W. Control growth of carbon nanofibers on Ni/activated carbon in a fluidized bed reactor. Microporous and Mesoporous Materials 131 (2010): 393–400.
- Guo, J., and Lua, A. C. Microporous activated carbons prepared from palm shell by thermal activation and their application to sulfur dioxide adsorption. Colloid and Interface Science 251 (2002): 242–247.
- Guo, S., et al. Effects of CO₂ activation on porous structures of coconut shell-based activated carbons. Applied Surface Science 255 (2009): 8443–8449.
- Guo, Y., et al. The preparation and mechanism studies of rice husk based porous carbon. Materials Chemistry and Physics 74 (2002): 320–323.

- Iglesia, E. Design, synthesis, and use of cobalt-based Fischer-Tropsch synthesis catalysts. Applied Catalysis A 161 (1997): 59-78.
- Ji, L., Lin, J., and Zeng, H.C. Metal-Support Interactions in Co/Al₂O₃ Catalysts: A Comparative Study on Reactivity of Support. The Journal of Physical Chemistry B 104 (2000): 1783-1790.
- Jiao, G., et al. Effect of La₂O₃ doping on syntheses of C₁–C₁₈ mixed linear α -alcohols from syngas over the Co/AC catalysts. Applied Catalysis A: General 364 (2009): 137–142.
- Kalderis, D., Bethanis, S., Paraskeva, P., and Diamadopoulos, E. Production of activated carbon from bagasse and rice husk by a single-stage chemical activation method at low retention times. Bioresource Technology 99 (2008): 6809–6816.
- Khodakov, A. Y., Chu, W., and Fongarland, P. Advances in the Development of Novel Cobalt Fischer-Tropsch Catalysts for Synthesis of Long-Chain Hydrocarbons and Clean Fuels. Chemical Reviews 107 (2007): 1692-1744.
- Kowalczyk, Z., et al. Supported ruthenium catalysts for selective methanation of carbon oxides at very low CO_x/H₂ ratios. Catalysis A: Applied General 342 (2008): 35-39.
- Kumar, A. G., et al. Immobilization of proteolytic enzyme on highly porous activated carbon derived from rice bran. Journal of Porous Materials 16 (2009): 439-445.
- Kusama, H., Bando, K. K., Okabe, K., and Arakawa, H. Effect of metal loading on CO₂ hydrogenation reactivity over Rh/SiO₂ catalysts. Applied Catalysis A: General 197 (2000): 255-268.
- Lahtinen, J., Anraku, T., and Somorjai, G. A. C, CO and CO₂ hydrogenation on cobalt foil model catalysts: evidence for the need of CoO reduction. Catalysis Letters 25 (1994): 241-255.

- Lee, G. D., Moon, M. J., Park, J. H., Park, S. S., and Hong, S. S. Raney Ni catalysts derived from different alloy precursors part II. CO and CO₂ methanation activity. Korean Journal of Chemical Engineering 22(4) (2005): 541-546.
- Li, W., et al. Effects of carbonization temperatures on characteristics of porosity in coconut shell chars and activated carbons derived from carbonized coconut shell chars. Industrial crops and products 28 (2008): 190-198.
- Liou, T. H., and Wu, S. J. Characteristics of microporous/mesoporous carbons prepared from rice husk under base- and acid-treated conditions. Journal of Hazardous Materials 171 (2009): 693-703.
- Lu, C. Y., and Wey, M. Y. The performance of CNT as catalyst support on CO oxidation at low temperature. Fuel 86 (2007): 1153-1161.
- Lu, C. Y., Wey, M. Y., and Chuang, K. H. Catalytic treating of gas pollutants over cobalt catalyst supported on porous carbons derived from rice husk and carbon nanotube. Applied Catalysis B: Environmental 90 (2009): 652-661.
- Lu, C. Y., Wey, M. Y., and Chen, L. I. Application of polyol process to prepare AC-supported nanocatalyst for VOC oxidation. Applied Catalysis A: General 325 (2007): 163-174.
- Ma, W. P., Ding, Y. J., and Lin, L. W. Fischer-Tropsch synthesis over activated-carbon-Supported cobalt catalysts: Effect of Co loading and promoters on catalyst performance. Industrial & Engineering Chemistry Research 43 (2004): 2391-2398.
- Matsuzaki, T., Takeuchi, K., Hanaoka, T., Arakawa, H., and Sugi, Y. Hydrogenation of carbon monoxide over highly dispersed cobalt catalysts derived from cobalt(II) acetate. Catalysis Today 28 (1996): 251-259.
- Pilecka, W. R., et al. Carbon-supported cobalt-iron catalysts for ammonia synthesis. Applied Catalysis A: General 300 (2006): 181-185.
- Pola, J., et al. IR laser-induced formation of amorphous Co-C films with crystalline Co, Co₂C and Co₃C nanograins in a graphitic shell. Journal of Photochemistry and Photobiology A: Chemistry 210 (2010): 153-161.

- Sun, S., Tsubaki, N., and Fujimoto, K. The reaction performances and characterization of Fischer–Tropsch synthesis Co/SiO₂ catalysts prepared from mixed cobalt salts. Applied Catalysis A: General 202 (2000): 121–131.
- Suo, Z., Kou, Y., Niu, J., Zhang, W., and Wang, H. Characterization of TiO₂-, ZrO₂- and Al₂O₃- supported iron catalysts as used for CO₂ hydrogenation. Applied Catalysis A 148 (1997): 301-313.
- Suzuki, R. M., Andrade, A. D., Sousa, J. C., and Rollemberg, M. C. Preparation and characterization of activated carbon from rice bran. Bioresource Technology 98 (2007): 1985-1991.
- Visconti, C. G., et al. Fischer–Tropsch synthesis on a Co/Al₂O₃ catalyst with CO₂ containing syngas. Applied Catalysis A: General 355 (2009): 61–68.
- Wang, T., Ding, Y., Lu, Y., Zhu, H., and Lin, L. Influence of lanthanum on the performance of Zr-Co/activated carbon catalysts in Fischer-Tropsch synthesis. Journal of Natural Gas Chemistry 17 (2008): 153–158.
- Wang, T., et al. Effect of vanadium promotion on activated carbon-supported cobalt catalysts in Fischer–Tropsch synthesis. Catalysis Letters 107 (2006): 47-52.
- Wang, L., Zhang, S., and Liu, Y. Reverse water gas shift reaction over Co-precipitated Ni-CeO₂ catalysts. Journal of rare earths 26 (2008): 66-70.
- Wei, S., Li, Z., and Yaping, Z. Preparation of microporous activated carbon from raw coconut shell by two-step procedure. Chinese Journal of Chemical Engineering 14(2) (2006): 266-269.
- Xiong, J., et al. The formation of Co₂C species in activated carbon supported cobalt-based catalysts and its impact on Fischer–Tropsch reaction. Catalysis Letters 102 (2005): 265-269.
- Xu, D., Dai, P., Guo, Q., and Yue, X. Improved hydrogen generation from alkaline NaBH₄ solution using cobalt catalysts supported on modified activated carbon. International Journal of Hydrogen Energy 33 (2008) 7371–7377.

- Yamasaki, M., Habazaki, H., Asami, K., Izumiya, K., and Hashimoto, K. Effect of tetragonal ZrO₂ on the catalytic activity of Ni/ZrO₂ catalyst prepared from amorphous Ni-Zr alloys. Catalysis Communications 7 (2006): 24-28.
- Zaman, M., Khodadi, A., and Mortazavi, Y. Fischer–Tropsch synthesis over cobalt dispersed on carbon nanotubes-based supports and activated carbon. Fuel Processing Technology 90 (2009): 1214–1219.
- Zhang, Y., Jacobs, G., Sparks, D. E., Dry, M. E., and Davis, B. H. CO and CO₂ hydrogenation study on supported cobalt Fischer–Tropsch synthesis catalysts. Catalysis Today 71 (2002): 411–418.
- Zhou, M., Wang, W., and Chi, M. Enhancement on the simultaneous removal of nitrate and organic pollutants from groundwater by a three-dimensional bio-electrochemical reactor. Bioresource Technology 100 (2009): 4662–4668.
- Zhu, Z., Lu, G. Q., Zhuang, Y., and Shen, D. A Comparative Study of N₂O Conversion to N₂ over Co/AC and Cu/AC Catalysts. Energy & Fuels 13 (1999): 763-772.



APPENDICES

ศูนย์วิทยทรัพยากร
จุฬาลงกรณ์มหาวิทยาลัย

APPENDIX A

CALCULATION FOR CATALYST PREPARATION

Calculation for the preparation of cobalt loading catalyst (20%Co/AC_X_Y)

Based on 1.00 g of catalyst used, the composition of the catalyst will be as follows:

Cobalt = 0.20 g

Activated carbon = 1.00 – 0.20 = 0.80 g

Atomic weight of Co is 58.93 g/mol

Molecular weight of $\text{Co}(\text{NO}_3)_2 \cdot 6\text{H}_2\text{O}$ is 291.03 g/mol

Cobalt 0.20 g was prepared from Cobalt (II) nitrate hexahydrate

$$\text{Cobalt (II) nitrate hexahydrate required} = \frac{\text{MW of } \text{Co}(\text{NO}_3)_2 \cdot 6\text{H}_2\text{O} \times \text{cobalt required}}{\text{MW of Co}}$$

$$\text{Cobalt (II) nitrate hexahydrate required} = \frac{291.03}{58.933} \times 0.2$$

$$= 0.9877 \text{ g}$$

ศูนย์วิทยทรัพยากร
จุฬาลงกรณ์มหาวิทยาลัย

APPENDIX B

CALCULATION FOR TOTAL CO CHEMISSORPTION
AND DISPERSION

Calculation of the total CO chemisorption and metal dispersion of the catalyst, a stoichiometry of CO/Co = 1, measured by CO chemisorption is as follows:

Calculation of total CO chemisorptions and active site

Let the weight of catalyst used	=	W	g
Integral area of CO peak after adsorption	=	A	unit
Integral area of 86 μ l of standard CO peak	=	B	unit
Amounts of CO adsorbed on catalyst	=	B-A	unit
Concentration of Co	=	C	%wt
Volume of CO adsorbed on catalyst	=	$86 \times [(B - A) / B]$	μ l
Volume of 1 mole of CO at 30°C	=	24.86	l
Mole of CO adsorbed on catalyst	=	$[(B - A) / B] \times [86 / 24.86]$	μ mole
Total CO chemisorptions	=		
		$[(B - A) / B] \times [86 / 24.86] \times [1 / W]$	μ mole/g cat

$$\text{Molecule of CO adsorbed on catalysts} = [(B - A) / B] \times [86 / 24.86] \times [6.02 \times 10^{23}] \mu \text{ molecule}$$

$$\text{Metal active site} = [(B - A) / B] \times [1.08 \times 10^{24}] \times [1 / W] \times [10^{-6}] \text{ site/g cat}$$

Calculation of %metal dispersion

Definition of % metal dispersion:

$$\text{Metal dispersion (\%)} = 100 \times [\text{molecules of Co from CO adsorption} / \text{molecules of Co loaded}]$$

Determined the % metal dispersion as follow:

$$\%D = S_f \times \left[\frac{V_{ads}}{V_g} \right] \times \left[\frac{m.w.}{\%M} \right] \times 100\% \times 100\% \dots \dots \dots (B.1)$$

Where

- %D = %metal dispersion
 S_f = stoichiometry factor, (CO on Co* =1)
 V_{ads} = volume adsorbed (cm³/g)
 V_g = molar volume of gas at STP = 22414 (cm³/mol)
m.w. = molecular weight of the metal (a.m.u.)
 %M = %metal loading

Example: %Dispersion of Co/AC H₃PO₄ 400

Calculation Volume Chemisorbed (V_{ads})

$$V_{ads}(\text{cm}^3/\text{g}) = \left[\frac{V_{inj}}{m} \right] \times \sum_{i=1}^n \left(1 - \frac{A_i}{A_f} \right) \dots \dots \dots (C.2)$$

Where:

- V_{inj} = volumn injected (cm³) = 86 μL=0.086 cm³
 m = mass of sample (g)
 A_i = area of peak i
 A_f = area of last peak

To replace values in equation (1) and (2);

$$\begin{aligned} V_{ads} &= \left[\frac{0.086}{0.0525} \right] \times \left[\left(1 - \frac{0.08343}{0.1674} \right) + \left(1 - \frac{0.15039}{0.1674} \right) + \left(1 - \frac{0.1571}{0.1674} \right) + \left(1 - \frac{0.16545}{0.1674} \right) + \left(1 - \frac{0.16546}{0.1674} \right) \right] \\ &= 1.127 \text{ cm}^3/\text{g} \\ \%D &= 1 \times \left[\frac{1.127}{22414} \right] \times \left[\frac{58.993}{17.4} \right] \times 100\% \times 100\% \\ &= 1.7 \% \end{aligned}$$

%Co dispersion is 1.7 %

APPENDIX C

CALCULATION OF TURNOVER OF FREQUENCY

Metal active site = y molecule/g catalysts

TOF = $\frac{\text{rate}}{\text{(number of active site)}}$

$$= \frac{[\text{molecule substrate converted}]}{[\text{g cat.}][\text{min}]} \left| \frac{[\text{g cat.}]}{y[\text{active site}]} \right| \frac{[\text{min}]}{[\text{s}]}$$

$$= [\text{s}^{-1}]$$

ศูนย์วิทยทรัพยากร
จุฬาลงกรณ์มหาวิทยาลัย

APPENDIX D

CALIBRATION CURVES

This appendix showed the calibration curves for calculation of composition of reactant and products in CO₂ hydrogenation reaction. The reactant is CO₂ and the main product is methane. The other products are linear hydrocarbons of heavier molecular weight that are C₂-C₄ such as ethane, ethylene, propane, propylene and butane.

The thermal conductivity detector, gas chromatography Shimadzu model 8A was used to analyze the concentration of CO₂ by using Molecular sieve 5A column.

The VZ10 column are used with a gas chromatography equipped with a flame ionization detector, Shimadzu model 14B, to analyze the concentration of products including of methane, ethane, ethylene, propane, propylene and butane. Conditions uses in both GC are illustrated in Table D.1.

Mole of reagent in y-axis and area reported by gas chromatography in x-axis are exhibited in the curves. The calibration curves of CO₂, CO, methane, ethane, ethylene, propane, propylene and butane are illustrated in the following figures.

Table D.1 Conditions use in Shimadzu modal GC-8A and GC-14B.

Parameters	Condition	
	Shimadzu GC-8A	Shimadzu GC-14B
Width	5	5
Slope	50	50
Drift	0	0
Min. area	10	10
T.DBL	0	0
Stop time	8	20
Atten	2	2
Speed	10	3

Method	1	1
Format	1	1
SPL.WT	100	100
IS.WT	1	1

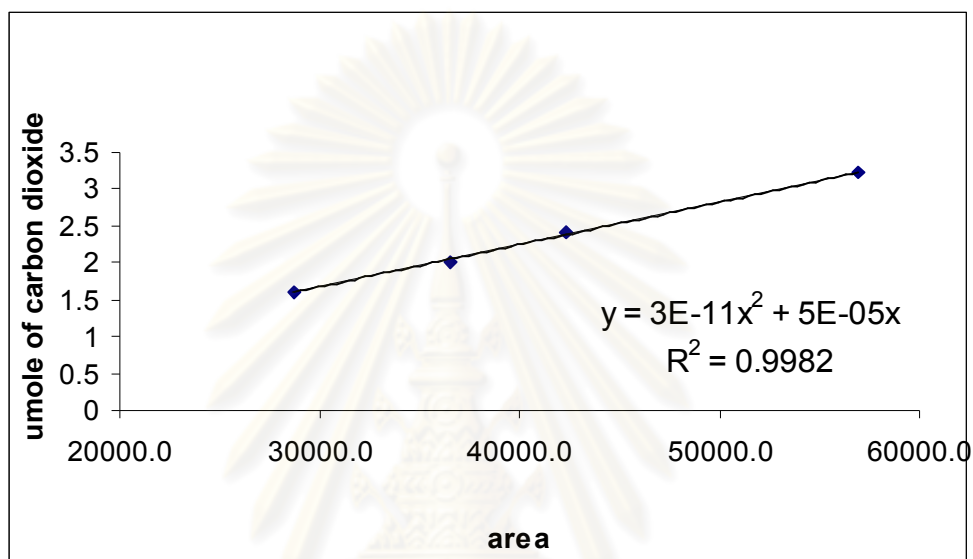


Figure D.1 The calibration curve of carbon dioxide.

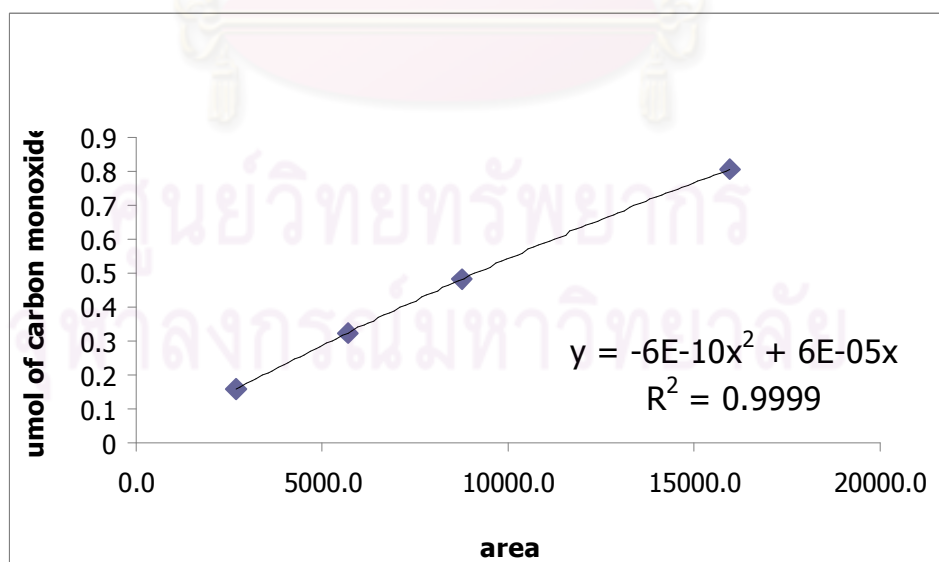


Figure D.2 The calibration curve of carbon monoxide.

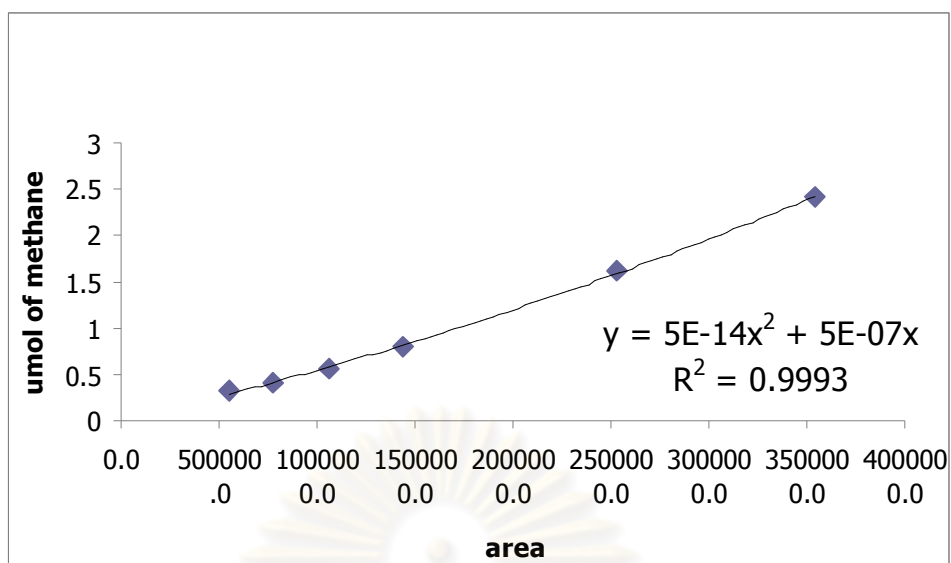


Figure D.3 The calibration curve of methane.

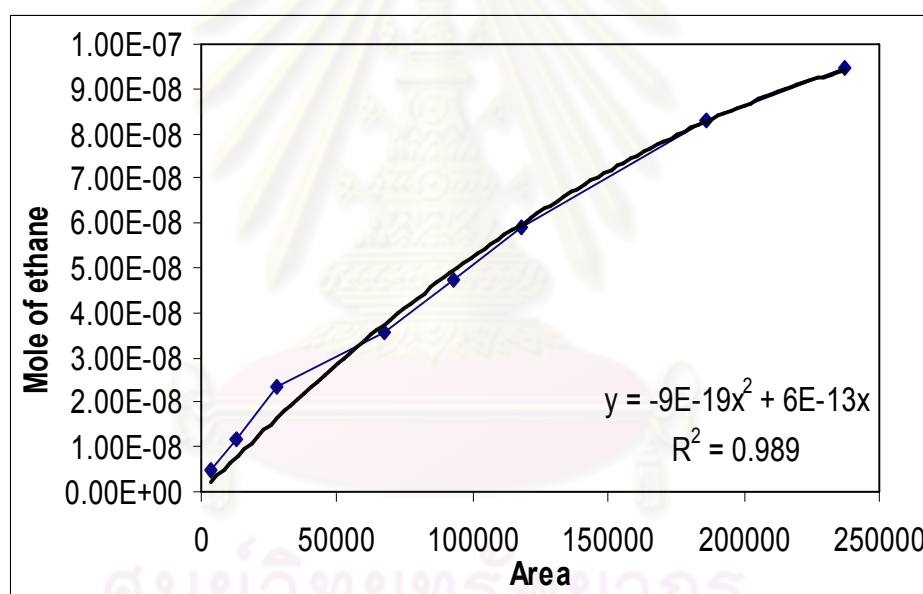


Figure D.4 The calibration curve of ethane.

APPENDIX E

CALCULATION OF CO₂ CONVERSION, REACTION RATE AND
SELECTIVITY

The catalyst performance for the CO₂ hydrogenation was evaluated in terms of activity for CO₂ conversion rate and selectivity.

Activity of the catalyst performed in term of carbon dioxide conversion and reaction rate. Carbon dioxide conversion is defined as moles of CO₂ converted with respect to CO₂ in feed:

$$\text{CO}_2 \text{ conversion (\%)} = \frac{100 \times [\text{mole of CO}_2 \text{ in feed} - \text{mole of CO}_2 \text{ in product}]}{\text{mole of CO}_2 \text{ in feed}}$$

Reaction rate was calculated from CO₂ conversion that is as follows:

Let the weight of catalyst used	=	W	g
Flow rate of CO ₂	=	2	cc/min
Reaction time	=	60	min
Weight of CH ₂	=	14	g
Volume of 1 mole of gas at 1 atm	=	22400	cc

$$\text{Reaction rate (g CH}_2\text{/g of catalyst)} = \frac{[\% \text{ conversion of CO}_2 / 100] \times 60 \times 14 \times 2}{W \times 22400}$$

Selectivity of product is defined as mole of product (B) formed with respect to mole of CO₂ converted:

$$\text{Selectivity of B (\%)} = 100 \times [\text{mole of B formed} / \text{mole of total products}]$$

APPENDIX F

REVERSE WATER GAS SHIFT (RWGS) REACTION



T. Osaki et al. studied kinetics of reverse water gas shift (RWGS) disulfide catalysts found that the hydrogenation of CO_2 on the disulfides of molybdenum and tungsten exhibited lower activities than the transition metals of Fe, Co, and Ni supported on Al_2O_3 , however, the selective hydrogenation of CO_2 to CO via the RWGS reaction was observed. A moderately strong affinity for H_2 rather than for CO_2 was observed on MoS_2 and WS_2 catalysts. The cause for the selective hydrogenation of CO_2 to CO was found to be due to the suppression of C-O bond breaking in CO molecule produced by the CO_2 hydrogenation. In addition, W. Luhui et al. studied reverse water gas shift reaction over Co-precipitated Ni-CeO₂ catalysts found that the main active sites for RWGS reaction were oxygen vacancies and highly dispersed Ni.

VITA

Mr. Benjapol Niticharoenwong was born on 23th May 1985, in Songkhla, Thailand. He received his Bachelor degree of Chemical engineering from Chulalongkorn University, Thailand in April 2009. Since May 2009, he has been studying for his Master degree of Engineering from the department of Chemical Engineering, Chulalongkorn University.

LIST OF PUBLICATIONS

Benjapol Niticharoenwong, Bunjerd Jongsomjit, Proceedings of the RSCE 2010 The 17th Regional Symposium on Chemical Engineering, Queen Sirikit National Convention Center, Bangkok, Thailand, November 22-23, 2010.

ศูนย์วิทยทรัพยากร
จุฬาลงกรณ์มหาวิทยาลัย